Chapter 2: Macroscopic Stability

Table of Contents

This page intentionally left blank

Chapter 2

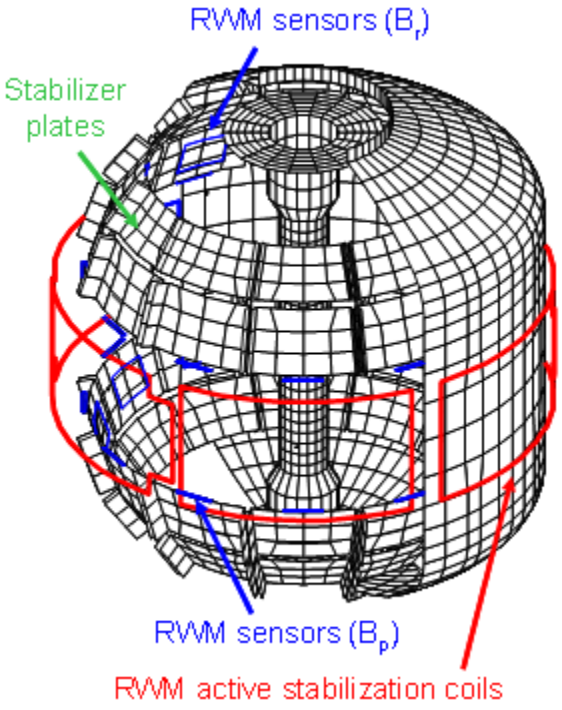

2 Macroscopic Stability

2.1 Maintaining High Beta Macroscopic Stability in the Spherical Torus

Economically attractive operation of a thermonuclear fusion reactor based on the tokamak magnetic confinement concept requires that the burning plasma maintain stability at high ratio of the plasma pressure to that of the confining magnetic field. Therefore, an important figure of merit for tokamak operation is the toroidal beta $\beta_t \equiv 2\mu_0\langle p\rangle/B_{t0}^2$ where $\langle p\rangle$ is the volume-averaged pressure and B_{t0} is the vacuum toroidal field at the plasma geometric center.

Stable high beta operation alone is insufficient for the tokamak design to yield an efficient steady-state reactor. Superior plasma equilibria will self-generate most, or all, of the plasma current via the pressure gradient driven neoclassical bootstrap effect, decreasing the auxiliary current drive power requirements. Since the bootstrap current is naturally driven closer to the plasma edge than the core, it creates broad

current profiles, and therefore equilibria with low plasma internal inductance, l_i. This leads to an apparent conflict of optimizing constraints, as tokamak experiments have shown that ideal magnetohydrodynamic (MHD) stability of large scale global modes with vacuum boundary ("no-wall") conditions decreases with decreasing l_i [1,2,3]. This beta limit is typically characterized by the normalized beta $\beta_N \equiv \beta_t(\%)a(m)B_0(T)/I_P(MA)$. Since $\beta_t \propto \beta_N^2$ at fixed bootstrap fraction and since fusion power output $P_{fus} \propto \beta_t^2 \propto \beta_N^4$, maximizing β_N is especially significant.

Tokamak research has shown that the inclusion of conducting wall ("wall-stabilized") boundary conditions can lead to stabilization of global MHD modes [4,5] with especially high values of β_N and β_N/l_i predicted by ideal MHD theory [6] for tokamak designs with low aspect ratio – the spherical torus (ST) [7]. However, reactor design studies show that the favorable promise of stable high β_N and low l_i ST equilibria must be a reality to create an efficient steady-state ST reactor [8]. Therefore, it was critical that such conditions first be demonstrated, with subsequent demonstration that the conditions be maintained.

NSTX has demonstrated the promise of advanced tokamak operation in a mega-Ampere class spherical torus, and in present and future research moves forward to demonstrate the reliable *maintenance* of these conditions. An illustration of the evolution to the high β_N and β_N/l_i wall stabilized state is shown in Figure 2.1-1 and Figure 2.2.1-2. Accessing this operational state was a long-term plan that was defined during the conceptual design of the device. A milestone in the process was reaching the ideal "no-wall" limit, which was achieved after neutral beam heating was installed on the device, as illustrated in Figure 2.1-1 (further detail published in Ref. 9). The figure as published illustrated the planned paths to higher β_N operation in the device; this path was successfully executed with NSTX wall-stabilized plasmas now having reached $\beta_N > 7$ and $\beta_N/l_i > 11$, as well as $\beta_t > 39\%$ - significant low aspect ratio advanced tokamak equilibria (Figure 2.2.1-2). Three key practical elements to this success were the reduction of the static error fields in the device, the routine access to broad pressure profiles via H-mode operation, and maintaining the minimum q value greater than unity [10]. Maintenance of sufficient plasma rotation was also found to be important to this success, and the impact of the rotation profile on MHD stability remains a subject of active research.

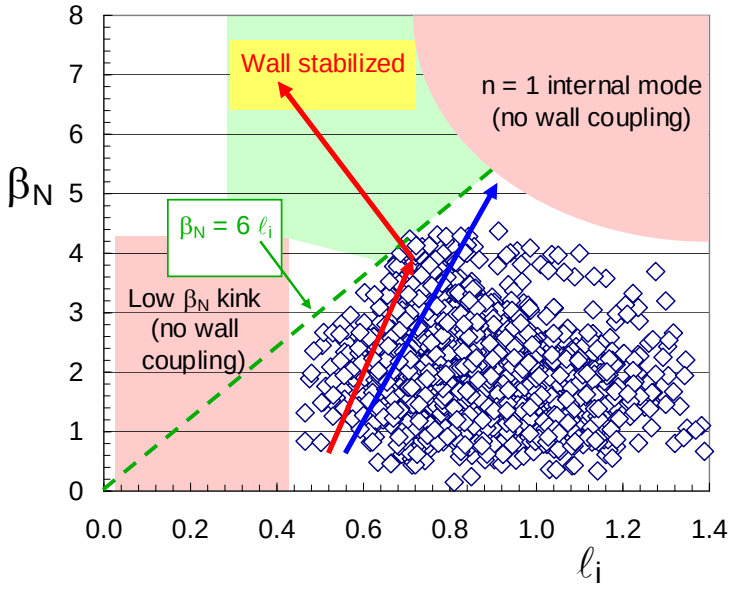

Figure 2.2.1-1 Early (l_i, β_N) stability space operational diagram for NSTX (from Sabbagh, et al., Phys. Plasmas 2002).

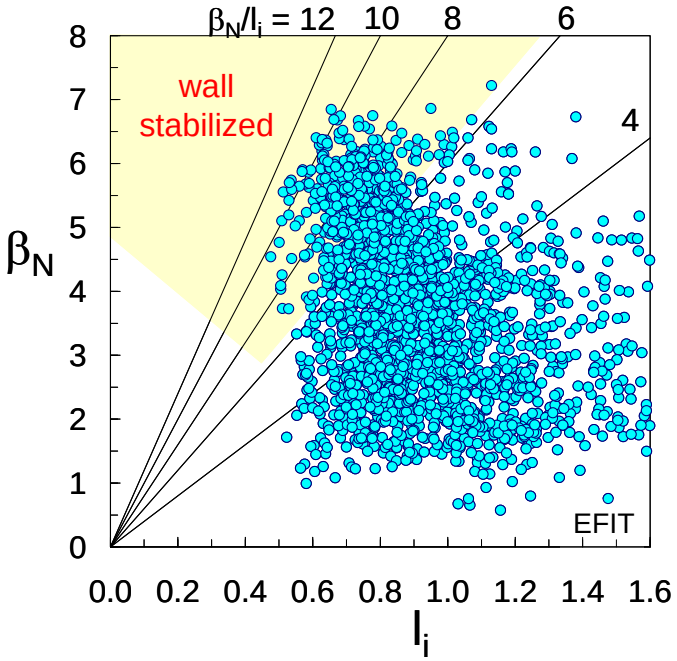

Figure 2.2.1-2 Wall-stabilized operation in NSTX at high $\beta_N > 7$, $\beta_N/l_i > 11$.

The high beta, low l_i equilibria created to date on NSTX are significant advances, especially because any one of several factors might have led to a failure to reach these operational states required for successful and efficient ST reactor or CTF operation. For example, the low l_i, high bootstrap fraction equilibria produced may not have been wall stabilized, or H-mode pressure profiles may not have been sufficiently broad to allow the high β_N operation shown in Figure 2.2.1-2. The NSTX research shows that the original theoretical plan came to pass experimentally. The stability challenges faced so far have been met, and have created important understanding in several areas including kink/ballooning and resistive wall mode (RWM) stabilization, the behavior of the n=1/m=1 mode, and long pulse operation including maintenance of $q > 1$ [2,9,11,12].

The overarching goal for MHD research in the 2009 – 2013 period – reliable maintenance of the highest beta conditions – is a key step to ST development, leads to a knowledge base of advanced tokamak research at all device aspect ratios, and naturally follows from the present NSTX database. Plasma shaping research has produced high beta and confinement performance in plasmas with high bootstrap current fraction. Both kink/ballooning stabilization and passive resistive wall mode stabilization have been demonstrated producing plasmas at least 50% above no-wall limit, $\beta_N^{no\text{-}wall}$. Accessing higher elongation (up to 3) and shaping factors has also required plasmas with lower l_i to maintain vertical stability. Sustained operation of high β_N in such plasmas in the next five years is expected to extend stabilization to higher ratios of $\beta_N / \beta_N^{no\text{-}wall}$. Understanding when and how such stabilization fails is now of paramount importance, including the role of plasma rotation magnitude and profile, Alfvén frequency, ion collisionality, ν_i, and aspect ratio. Active RWM stabilization has just begun on the device, with the key focus now on maintaining this stabilization indefinitely. Dynamic error field correction (DEFC) has shown sufficient effectiveness to maintain or slightly increase stabilizing plasma rotation, and will continue to be developed to maintain or increase plasma beta and confinement performance. The occurrence and impact of neoclassical tearing modes in low aspect ratio geometry will be investigated, including the dependence of mode onset on rotation, rotation shear, and bootstrap drive, the source of NTM triggering when $q_{min}>1$, and fast particle redistribution. First-principles understanding of plasma rotation damping achieved in the last five years on NSTX will be tested further, examining for example the dependence on ion collisionality. This understanding can be used to generate the new techniques for maintenance or increase of plasma rotation that are proposed for the coming five year period. Disruption

studies will also be expanded in NSTX, examining important technical detail such as halo current generation, thermal and current quench studies, and first wall power distribution for future burning plasma devices.

It is expected that the planned NSTX MHD research for the 2009 – 2013 period in all of the areas proposed and roughly outlined above will benefit significantly from joint experiments with toroidal magnetic confinement experiments including MAST and DIII-D. The strength in joint MAST / NSTX experiments hinges on the uniqueness of the ST operating space (e.g. ultra-high beta approaching unity in the core plasma) while examining differences due to machine configurations. For example, comparison of global mode stability in MAST and NSTX will lead to further understanding the role of the conducting wall and plasma rotation in stabilization. A joint experiment to study neoclassical toroidal viscosity has been proposed to be run in 2008. The strength in joint experiments between NSTX and DIII-D hinge upon the complementarity of the devices. Examples of this include the large difference in Alfvén frequency (applicable to RWM stability theory) and the explicit aspect ratio dependence that appears in most neoclassical effects including NTM stabilization, RWM stability theory, and non-resonant plasma viscosity theory. Joint experiments have already been conducted between NSTX and DIII-D in the RWM topical area [13], and experiments in the 2007 and 2008 run periods have started joint research in the NTM area.

Note that MHD research during the 2009 – 2013 period in the important area of energetic particle modes will be covered in Chapter 4 of this document “Waves and Energetic Particles” and ELM stability will be covered in Chapter 5 “Boundary Physics”.

2.2 Overview of Research Plans for FY2009-2013

MHD research on NSTX has produced high beta plasmas yielding several classes of beta-limiting instabilities. With transient beta goals established, and RMW/kink instabilities observed and documented, the natural emphasis of MHD research turns to (i) the physical understanding of beta-limiting and other deleterious modes and methods of stabilizing them and (ii) controlling these modes either directly or indirectly, while understanding the physics explaining this control. Another important approach to understanding and producing mode stabilization is through control of the underlying equilibrium profiles.

Two such areas to be addressed further in the coming five year period are the control of the plasma rotation and *q* profiles. This research applies to the ST development path toward future burning plasma devices and has direct application to the understanding of tokamak mode stabilization in general. The research utilizes the unique and complementary aspects of the advanced tokamak equilibrium produced in NSTX, including very high beta, low aspect ratio, and low l_i to leverage the validation of physical theories of key phenomena.

2.2.1 Long-term Research Goal

Demonstrate high reliability, sustained operation of high confinement, high beta low aspect ratio tokamak plasmas operating near the computed ideal, with-wall β_N limit by gaining an understanding of the underlying mode stabilization physics and implementing appropriate control techniques.

2.2.2 General Objectives of Macroscopic Stability Research

NSTX Macroscopic Stability research comprises two general objectives that support the long-term goal:

(OBJECTIVE 1) *advancement of the physics understanding of low aspect ratio, high beta tokamak plasma devices in support of a development path to sustained fusion generation in future devices*

NSTX has pioneered the operation of low aspect ratio, high beta plasma equilibria in a mega-ampere class device and has demonstrated ultra-high beta operation with high energy confinement. Several crucial and favorable physics results have resulted in a successful proof-of-principle demonstration of the low aspect ratio spherical torus concept as the baseline for a next-step device. The generation of relatively broad pressure profiles in H-mode operation increases MHD stability limits. The broad current profiles (low l_i) of high performance equilibria yield superior alignment of the bootstrap current profile and open a large conducting wall-stabilized operating space. Sufficient plasma rotation induced by neutral beam injection affords passive RWM stabilization, allowing operation of the device at maximum β_t and β_N. The plasmas created to date in NSTX are advanced tokamak equilibria that were only envisioned (and highly desired) theoretically during the past period of conventional tokamak operation. CTF designs based on the ST can

expect with greater confidence the ability to operate at pressure and confinement levels required to meet fusion performance goals. The 2009 – 2013 research period in NSTX aims at solving key issues related to reliable long-pulse operation of these high beta equilibria, including operation at ultra high elongation (~ 3), RWM stabilization, NTM physics, maintenance of stabilizing plasma rotation, and an improved understanding of disruption physics, prediction, and mitigation techniques.

(OBJECTIVE 2) *applied stability physics understanding applicable to tokamaks in general, leveraged by the unique low aspect ratio and high beta operational regime of the device*

The key to successful extrapolation of techniques used in present tokamak experiments to future burning plasma devices is a first-principles understanding of the underlying physics. A powerful tool in this endeavor is the ability to test physics hypotheses in significant and different operational regimes. NSTX offers the ability for researchers to fully test key physics hypotheses in an operational space not accessible in other devices, for example in the important scaling parameters of beta and aspect ratio, which appear prominently in MHD stability theory and neoclassical transport theory. Having this unique and complementary ability to test key theories allows greater confidence in extrapolating theory to future devices, thereby reducing both risk and development time in the goal of fusion energy development.

2.2.3 Top-level Research Goals by Topical Area

- *High plasma elongation sustainment and global stability*

  Goal: *sustain stable, high beta operation at very high plasma elongation ~ 3 as a proof-of principle for ST development and to confirm MHD stability theory in this operating space.*

- *Resistive wall mode control and stabilization physics*

  Goal: *Determine the physics of RWM stabilization, by both passive and active means, and apply this understanding to optimize and increase reliability of active stabilization in low aspect ratio plasmas. Use this information to provide greater confidence in models used to extrapolate RWM stabilization performance to future tokamaks including burning, and driven-burn plasma devices such as ITER and ST-CTF.*

- *Dynamic error field correction*

  Goal: *Determine sources of dynamically changing error field due to inherent asymmetries in the device and the plasma physics responsible for amplification of these sources. Apply techniques that will dynamically cancel these fields to maintain plasma rotation and stability.*

- *Tearing Mode / NTM physics*

  Goal: *Study neoclassical and classical tearing modes in the unique low aspect ratio, high beta, and large ion gyro-radius plasmas available in NSTX, in order to both extrapolate our understanding to future ST devices and provide data complementary to that from conventional aspect ratio tokamaks. Investigate the impact of these modes on plasma beta, rotation, fast particle redistribution, and the potential of low aspect ratio operation as being theoretically favorable for NTM stability. Determine scenarios that allow operation without these deleterious instabilities.*

- *Plasma rotation and non-axisymmetric field-induced viscosity*

  Goal: *Continue to develop quantitative, first-principles physics models of non-axisymmetric field induced plasma viscosity for both resonant and non-resonant field, and apply results to create new techniques for imparting significant toroidal momentum to the plasma.*

- *Disruption physics, consequences, avoidance, and prediction*

  Goal: *Characterize the effects of disruptions at low aspect ratio and high beta by measuring halo currents, and thermal and current quench characteristics. Develop methods to predict disruptions and mitigate their impact.*

2.2.4 Overview of Major Device Upgrades Supporting Planned Research

Several device upgrades (See Chapter 7) to NSTX will strongly support the goal of reliably sustained high beta operation with physics understanding for confident extrapolation toward a driven-burn ST-CTF. As discussed throughout this chapter, a critical element for testing stabilization physics of all beta-limiting modes and plasma rotation damping is operation at lower ν_i. This will be afforded by an upgrade to the device center column that will allow a doubling of the toroidal field to the typical high field operational value of 0.5 T to 1.0 T and an increase in plasma current from a typical value of 1 MA to 2 MA. As the energy confinement time in NSTX scales favorably with both B_t and I_p, plasma stored energy could quadruple, exceeding 1 MJ, and ν_i could decrease by an order of magnitude (Figure 2.2.4-1), to within a factor of 2 of the proposed NHTX (Section 1.4.1) device. This is especially important as neoclassical effects are expected to be amplified in this transition region from weakly to strongly collisionless operation. For example, the dependence of RWM stabilization (Section 2.3.2) and neoclassical toroidal viscosity on ν_i (Section 2.3.5) can be tested at levels closer to an ST-CTF.

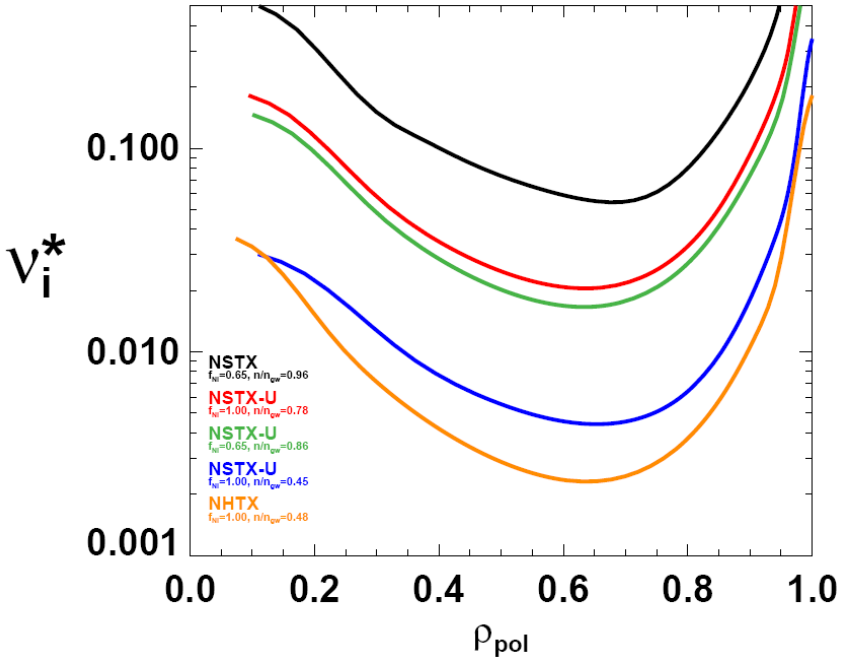

Figure 2.2.4-1 Profiles of the ion collisionality to bounce frequency ratio from TRANSP for an existing NSTX plasma (116313) compared to significantly reduced levels predicted for NSTX-U and NHTX at various non-inductive current fractions and Greenwald density ratios.

The addition of a second neutral beam source, planned for operation at the end of the five year plan period, will provide critical capabilities including alteration of the *q* profile to study the effects on MHD modes, especially NTMs, with a goal of stabilizing deleterious modes at elevated $q > 2$ (see Section 6.3.2 and Figure 6.3.3 for *q* profile calculations for the upgrade). It will also provide greater ability to produce highly non-inductive high β plasmas that will be sustained for several seconds – suitable targets to demonstrate suppression or control of instabilities. A set of off-midplane non-axisymmetric control coils (NCC) are also planned (with incremental funding) to supplement the existing midplane control coils (see Section 2.3.2.1). These coils will serve several roles on NSTX including ELM and RWM control, and would provide important supporting research for ITER as the envisioned coil geometry closely resembles the present ITER VAC02 coil design (endorsed by the ITER Science and Technical Advisory Committee). Finally, very recent operation of NSTX with lithium evaporation on plasma facing components has demonstrated suppression of ELMs and mitigation of NTMs – a remarkable result for which the stability physics is yet to be understood. A phased plan of liquid lithium divertors (LLD - starting in 2009) has therefore become an important tool to better understand the underlying physical cause of MHD mode stabilization and to determine if the LLD is more or less effective in this role compared to the present lithium deposition system (LITER). Suppression of ELMs and NTMs eliminates energy dissipation by these modes, making them more susceptible to both resonant field amplification (RFA) by stable RWMs, and unstable RWMs, emphasizing the need for reliable feedback control of these modes in these conditions.

2.2.5 Guidance for Macroscopic Stability Research Goals

Guidance for NSTX MHD research has always been closely linked to the needs of the ST development and general tokamak objectives as embodied in directives set by major US and world advisory committees. The 5 year plan for 2004-2008 followed IPPA guidelines. At present, the major research topical areas defined by the Fusion Energy Science Advisory Committee (FESAC) are followed. In 2008 the FESAC Toroidal Alternates Panel was formed and recently, with input from the ST community and the DOE Spherical Torus Coordinating Committee (STCC), has formulated a U.S. ST mission to "develop a compact, high beta, burning plasma capability for fusion energy", and an ITER-era (20 year)

goal "to establish the ST knowledge base to construct a low aspect-ratio fusion component testing facility that provides high heat flux, neutron flux, and duty factor needed to inform the design of a demonstration fusion power plant".

The long term research goal and objectives stated in Sections 2.2.1 and 2.2.2 directly support this mission and goal, as CTF designs show that producing sufficient levels of fusion neutron fluence requires high β_N operation approaching or above the ideal no-wall beta limit, and high duty factor requires steady high β_N operation with few or no disruptions. Specific, detailed guidance is provided to the NSTX Research Team in several ways, and at the yearly NSTX Research Forum, the team defines the prioritized research experiments for a run period consistent with U.S. fusion program goals. Experiments receiving the highest run priority in 2007 - 2008 addressed the largest subset of the following guidelines:

1) NSTX DOE milestones
2) ST physics – research to directly support the development of the ST
3) ITPA / BPO – research that serves stated ITPA joint experiments and USBPO initiatives
4) ITER issue cards – research supporting ITER issue cards (for 2007)
5) Joint experiments with other US facilities

2.3 Macroscopic Stability Results and Plans by Topical Area

The balance of the document states present research results and plans by topical area stating (i) the goal of the research, (ii) present results of stability physics and control, (iii) research plans for the upcoming 5 year period, and (iv) a summarized timeline of the 5 year research plan.

2.3.1 High plasma shaping sustainment and global stability

Goal: *sustain stable, high beta operation at very high plasma elongation ($\kappa \sim 3$) and shaping as a proof-of principle for ST development and to confirm MHD stability theory in this operating space.*

(i) physics and control - results

The compact device size of an ST fusion reactor [14] or Component Test Facility [15] makes these devices attractive as it leads to a relatively low cost device compared to higher aspect ratio tokamaks. To optimize the efficiency of the system, it is crucial to run the device with high bootstrap current fraction f_{bs} and high β_t. Maximizing these parameters is equivalent to maximizing β_N and the plasma shaping parameter $S_I \equiv q_{95}(I_p/aBt)$ since $f_{bs}\beta_t \sim S_I\beta_N^2$ [16].

During the past five year period, a plan was executed to expand the initial equilibria created in the device [17] toward higher elongation and S_I [18]. The plasma control system (PCS) response time was improved to better control vertical instability, a substantial upgrade to the magnetic field sensors in the divertor region was made, real-time plasma boundary shape reconstruction (rtEFIT) was implemented to enable more accurate control of plasmas with higher S_I, and the center stack shaping coil PF1A was modified to allow the creation of high triangularity, δ, simultaneous with high elongation, κ. The combined increase of these two parameters is required to produce the greatest increase in ideal MHD stability. Also, δ has a much stronger effect on S_I at low aspect ratio than at high aspect ratio [19]. The PF1A coil modification is illustrated in Figure 2.3.1-1.

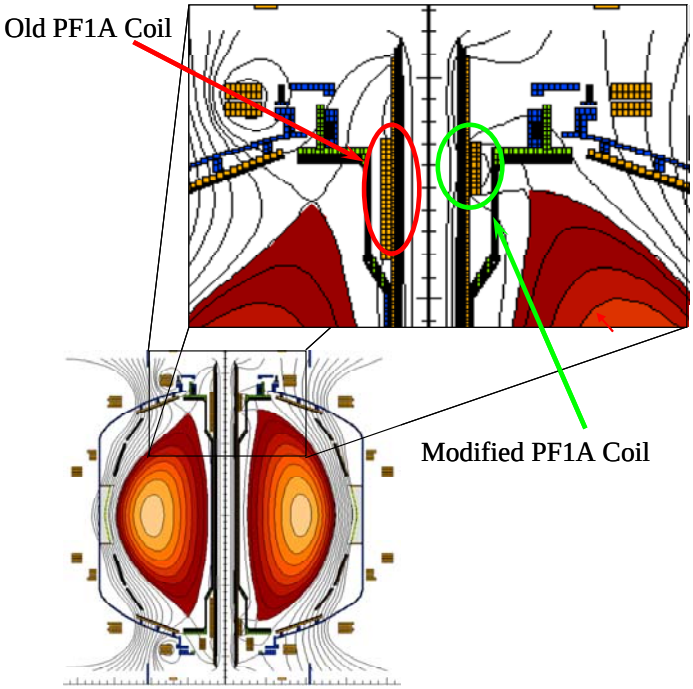

Figure 2.3.1-1 Upgrade of PF1A coil has enabled simultaneous achievement of high κ and δ.

The successful expansion of the NSTX operating space in κ and δ due to these improvements is summarized in Figure 2.3.1-2. Shots shown in the 2001 – 2003 period pre-date the improvements described above. As shown, the operating space was limited to $\kappa \sim 2.2$, with a small decrease from this value at the highest $\delta \sim 0.85$. The reduced latency of the PCS in 2004 led to a substantial increase in κ at intermediate $\delta \sim 0.6$. Finally, the PF1A coil upgrade (2005 – 2006 period shown) allowed access to high $\kappa > 2.5$ and high $\delta > 0.8$ simultaneously. Poloidal flux contours from equilibrium reconstructions illustrating this evolution and the increase in S_I attained are shown in Figure 2.3.1-3.

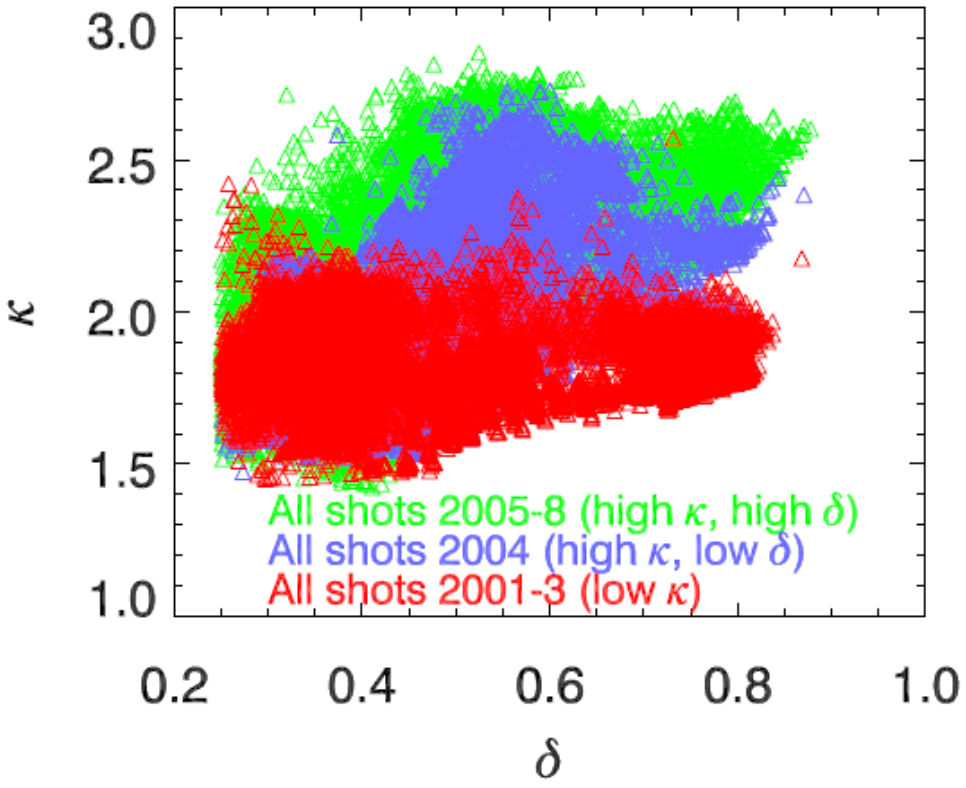

Figure 2.3.1-2 Expansion of NSTX operating space in κ and δ due to improvements made in the last five year period. Each point represents an EFIT equilibrium reconstruction. Data span the entire NSTX database and are filtered to avoid equilibria exhibiting rapid plasma motion.

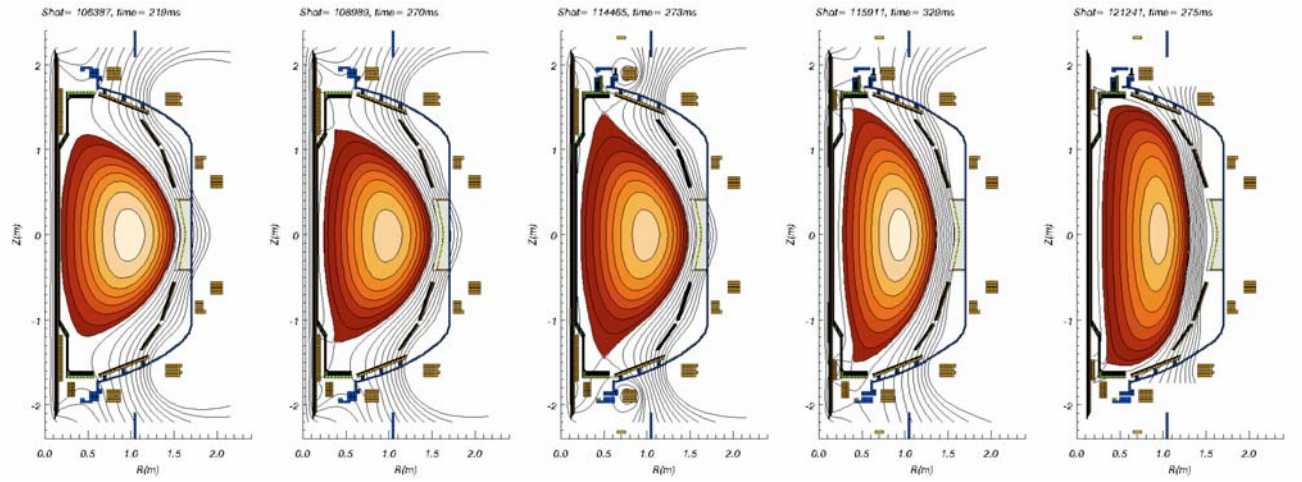

Figure 2.3.1-3 Evolution of plasma shaping capability in NSTX in the last five year years. From left to right (initial device capabilities 2001: κ = 1.8, δ = 0.6, S_I ~ 22; 2002-3: κ = 2.0, δ = 0.8, S_I ~ 23; PCS latency reduced 2004: κ = 2.3, δ = 0.6, S_I ~ 27; PF1A modification 2005: κ = 2.75, δ= 0.8, S_I ~ 37; 2006: κ = 3, δ= 0.8, S_I ~ 41.

While the high S_I equilibria have now been produced in NSTX, the initial plasmas somewhat unexpectedly displayed β_N limits close to the computed ideal MHD no-wall stability limits β_N ~ 4, rather than the values reached in wall-stabilized plasmas β_N ~ 6.5. This finding naturally called out the possibility that these plasmas have somehow lost passive kink/ballooning stabilization [18]. One possibility at sufficiently low l_i, as shown in Figure 2.2.1-2, is the destabilization of the purely current-driven kink mode, which eventually becomes unstable for all β_N when the edge current instability drive is sufficiently large. Investigating this possibility may lead to further understanding of the physics of passive stabilization of these modes. Another possibility is that the resistive wall mode (RWM) is destabilized in the high S_I plasmas since their larger size moves them closer to the conducting wall, and the RWM becomes *less* stable as the plasma is brought closer to the wall [20]. Another hypothesis being considered is the possibility of impurity-driven tearing modes.

Extension of high S_I plasmas to high β_N

Generating stable high S_I plasmas at high β_N is an important goal toward demonstrating that future devices such as an ST-CTF have sufficient margin against instability and the ability of sustaining plasma current non-inductively with a high fraction of bootstrap current. As such, these plasmas are of high

interest to several topical areas including MHD, which research will focus on access to, and maintenance of the wall-stabilized state with $\beta_N > 6$.

Recent experiments in this regard were conducted in June 2008 after lithium was deposited in the device and utilizing both active $n = 1$ RWM control and $n = 3$ DC error field correction. High elongation plasmas were created that have now reached β_N up to 6. These plasmas have low l_i, ~ 0.4 – 0.5 and may have significantly reduced core current (current holes). Further analysis of these recent experiments and comparison to the 2007 database is underway to determine the underlying physics responsible for accessing high β_N. Kink/ballooning and RWM stability will be investigated for these equilibria, especially the comparison of passive stabilization in these plasmas as compared to plasma with lower S_I and the reduced β_N. Potential differences in equilibrium profile shape including rotation will be examined.

(ii) physics and control - plans

Plasma control system upgrades

The general plan for upgrading the control capability of NSTX in the 2009 – 2013 period is substantial (β control upgrade, ELM mitigation/control upgrade, RWM stabilization/DEFC system upgrade, plasma rotation control upgrade, q profile alteration by second NBI). The upgrades for plasma boundary shaping are relatively minor, involving hardware changes required to support the center stack upgrade and associated software tasks. A new set of PCS control computers were successfully tested at the end of the 2007 run and used in 2008 with the upgrades to PCS software including more flexible n = 1 feedback system control. These computers run a LINUX operating system and have reduced the system latency by a factor of 2 compared to that in 2006 & 2007. Interfaces for planned β feedback control using real-time EFIT computation of β_N and NBI power for control were installed in 2008. Testing of this system will occur over the next year using an imposed target-beta specifications. A more sophisticated option for stability limit detection is real-time, low frequency MHD spectroscopy [21].Another important upgrade of the shaping control system will be to provide greater accuracy and reliability in strike point control for the new liquid lithium divertor to be installed. More details regarding these control upgrades can be found in chapter 7.

The overall goal of the 2009 – 2013 period hinges on research enabling the reliability and control of high beta ST plasmas. Real-time measurement of plasma rotation from charge exchange recombination spectroscopy (CHERS) for rotation control and real-time motional Stark effect data for real-time evaluation of the safety factor are planned. The latter would be used in real-time EFIT, allowing greater flexibility in the reconstructed current profile basis function set and evaluation for future q profile control. Alteration of the q profile will be possible with the addition of the second neutral beam line, with transport code predictions showing a large variation in core q values and q_{min} exceeding 3 (see Section 6.3.2 and Figure 6.3.3). The use of diagnostic and control algorithm upgrades to evaluate and/or allow feedback control of various plasma parameters for MHD studies are discussed further in the appropriate sections of this document. Examples of these include real-time rotation measurements using CHERS (section 2.3.5), LQG controllers for resistive wall mode stabilization (section 2.3.2), soft X-ray detection of RWMs for future use in the active control system (section 2.3.2), and implementation of disruption prediction/mitigation measures (section 2.3.6).

SUMMARY OF RESEARCH PLANS AND TIMELINE

FY2009-10 Test β feedback control real-time EFIT and NBI power for control. Conduct experiments to extend high S_I plasmas into wall-stabilized, high $\beta_N > 6$ operating space.

FY2010-12 Implement strike point control for liquid Li divertor experiments. Implement real-time measurement of plasma rotation. Begin initial rotation profile control experiments.

FY2012-13 Implement real-time MSE for evaluation of q. Attempt q_0 control with either HHFW current drive or second NBI (depending on hardware availability). Attempt beta feedback using simple (β_N, l_i, F_p) models and evaluate more sophisticated models. Demonstrate sustained high $\beta_N \sim 6$ in high elongation, highly shaped plasmas with newly upgraded center stack.

2.3.2 Resistive wall mode control and stabilization physics

Goal: *Determine the physics of RWM stabilization, by both passive and active means, and apply this understanding to optimize and increase reliability of active stabilization in low aspect ratio plasmas. Use this information to provide greater confidence in models used to extrapolate RWM stabilization performance to future tokamaks including burning, and driven-burn plasma devices such as ITER and ST-CTF.*

2.3.2.1 Active feedback control

(i) physics and control - results

Mode detection and control coils

Resistive wall modes are kink/ballooning modes whose growth is slowed by stabilizing conducting structures which allow control of the modes. Resistive wall modes are deleterious to sustaining plasma beta, in that unstable modes cause rapid β-collapses, loss of H-mode, and eventual plasma disruption. Weakly damped stable modes can cause resonant field amplification that can also facilitate disruptions by reducing plasma rotation, causing the plasma to be more susceptible to tearing mode locking.

Significant progress has been made regarding RWM stabilization physics and mode control in NSTX. Key to this success was the addition of new hardware capability to both diagnose and actively stabilize the RWM, and to alter the plasma rotation magnitude and profile. NSTX is equipped with 48 toroidally segmented copper conducting plates, covered with plasma facing carbon tiles, to provide kink-ballooning mode stabilization (**Figure 2.3.2-1**). These plates are arranged symmetrically in four toroidal rings, two above and two below the device midplane. The segments are independently connected to the stainless steel vacuum vessel by high resistance supports. Detection of the RWM is primarily made by magnetic loops measuring the radial, B_r, and poloidal, B_p, flux located at each of the plates closest to the midplane.

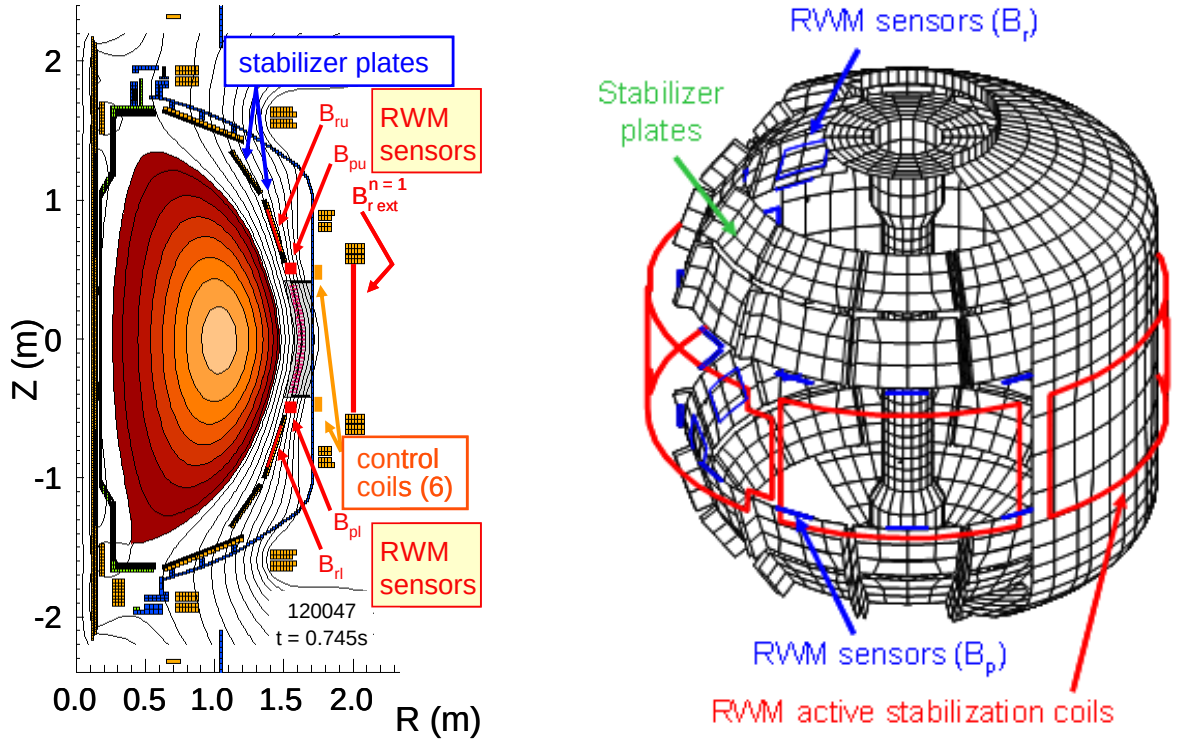

Figure 2.3.2-1 Diagram of NSTX conducting structure showing internal B_r and B_p sensors, passive stabilizing plates, and ex-vessel non-axisymmetric (RWM) control coils.

The B_r sensors are mounted between the carbon tiles and the copper shells, and the B_p sensors are mounted a few centimeters below each plate. The sensors are instrumented to detect modes with frequencies up to 2.5 kHz, sufficient to detect RWM growth and rotation frequencies in NSTX ($1/\tau_w$ ~ 200 Hz). The signals are processed to measure toroidal mode number, n, up to 3. The non-axisymmetric coil set, known as the RWM coil set, is comprised of six control coils located at the outboard midplane (**Figure 2.3.2-1**). Each coil has two turns, spans approximately 60 degrees of toroidal angle, and is located outside, but closely coupled to the device vacuum vessel. These coils have been primarily connected in diametrically-opposed, anti-series pairs that allow generation of odd parity n = 1 and 3 magnetic fields. Each coil pair is powered by an independent switching power amplifier capable of operation up to 3.3 kA at 7.5 kHz. This current corresponds to 10-15 G of n = 1 midplane radial field at the q = 2 surface. The fields generated by these coils can be used to reduce or amplify static and dynamic error fields, control ω_ϕ, and actively control the RWM.

Stabilization performance, resonant field amplification, and n > 1 observation

At the start of the last five year period, the n = 1 RWM had been identified as a discharge-terminating instability in the device [10]. The presence of large error fields resulted in unstable RWM growth soon after β_N exceeded $\beta_N^{no\text{-}wall}$, indicating reduced passive stabilization in this condition. In the last five year period, error field reduction and the increased maintenance of sufficient plasma rotation resulted in a much larger stabilized operating space, with $\beta_N/\beta_N^{no\text{-}wall}$ up to 1.5, producing the highest β_N achieved in the device [22]. The proximity of the plasma β_N to $\beta_N^{no\text{-}wall}$ was computed for the entire plasma discharge as desired with the DCON code [23] using reconstructed plasma equilibria that included kinetic profile data. This capability was available between shots in the NSTX control room. Maintaining high toroidal rotation across the entire profile produced passive RWM stabilization for long durations exceeding the eddy current decay time of the stabilizing plates of the device by at least a factor of 50 [24]. Pressure-driven amplification of applied non-axisymmetric fields was identified as resonant field amplification (RFA) [25] as had been identified in DIII-D [26,27]. The dependence of RFA on n = 1 applied field frequency and propagation direction with respect to the toroidal plasma rotation in NSTX showed the RFA to be due to weakly damped RWMs [22]. The RWM sensor system on NSTX was outfitted to discriminate both amplitude and phase of RWM mode activity with toroidal mode number between 1 – 3, and for the first time in a tokamak, the unstable RWM with n > 1 was observed [22] (Figure 2.3.2-2). The ideal MHD eigenfunctions with n = 1 – 3 were computed using the DCON code using reconstructed equilibria from this plasma discharge. By using the measured n = 1 – 3 mode amplitudes and phases, these eigenfunctions were scaled and summed in the proper phase to reconstruct the RWM field perturbation. This reconstruction is shown in Figure 2.3.2-3 Visible light emission (a) and DCON computed normal perturbed field (b,c) for the unstable RWM shown in Figure 2.3.2-2. (discharge 114147) at t = 0.268s. Along with the visible light observed from the plasma during the unstable RWM.

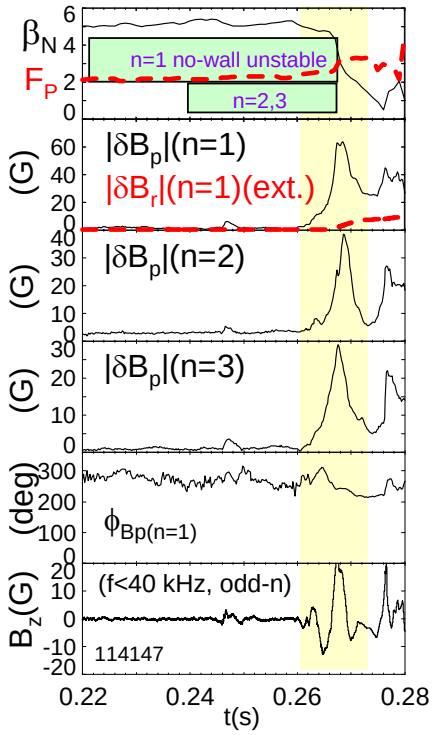

Figure 2.3.2-2 RWM toroidal mode spectrum and dynamics. The evolution of β_N, pressure peaking factor, F_p (dashed line), amplitude of n = 1-3 components of mode-generated B_p (internal to vacuum vessel), n=1 B_r (external to vacuum vessel; dashed line), phase of n = 1 mode-generated B_p, and integrated pickup loop data measuring the vertical field, B_z, for odd-n MHD modes are shown. The computed ideal MHD no-wall stability for n = 1-3 is also shown.

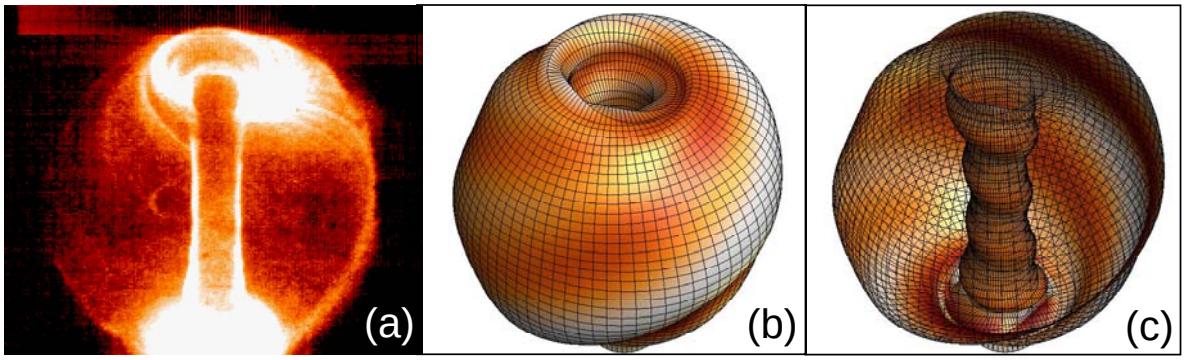

Figure 2.3.2-3 Visible light emission (a) and DCON computed normal perturbed field (b,c) for the unstable RWM shown in Figure 2.3.2-2. (discharge 114147) at t = 0.268s.

Active stabilization

Successful operation of the RWM active control system has demonstrated for the first time active stabilization of the pressure-driven RWM in high beta, low aspect ratio tokamak plasmas, with ω_ϕ significantly below the experimentally determined critical rotation profile for the chosen target plasma. A comparison of high β_N plasmas with and without RWM active stabilization is shown in Figure 2.3.2-4. The plasma without active stabilization has $\beta_N = 4.1$ as $\omega_\phi/2\pi$ at major radial position $R = 1.323$m (near the $q = 2$ flux surface) drops to below 4 kHz. At this time, RWM passive stabilization becomes insufficient and the $n = 1$ RWM becomes unstable, indicated by poloidal and radial field sensors (ΔB_p, $\Delta B_{r\text{-}ext}$), and β_N collapses. With active stabilization turned off, the current in one of three control coil pairs, I_A, is the pre-programmed $n = 3$ braking field current (Figure 2.3.2-4(c)). The experimentally fitted $n = 1$ RWM growth rate is between 0.5 – 0.25 s^{-1}. This agrees well with the theoretical growth rate $\gamma_{RWM} = 0.37$ s^{-1} as computed by the VALEN code [28], using experimental equilibrium reconstructions [17] including internal magnetic field pitch angle constraints from a motional Stark effect diagnostic. In contrast, the plasma with active stabilization does not suffer an unstable RWM and continues to increase in β_N up to 5.6 and β_t up to 19.4%, as ω_ϕ continues to decrease to $\omega_\phi/\Omega_{crit} = 0.2$ near $q = 2$. The RWM is actively stabilized above $\beta_N^{no\text{-}wall}$, as computed by the DCON MHD stability code [29], and below Ω_{crit} for a significantly long duration exceeding $90/\gamma_{RWM}$ and seven τ_E. The control coil current is now the superposition of $n = 3$ braking field current and $n = 1$ active feedback stabilization current, determined from the measured $n = 1$ RWM amplitude and phase. This amplitude, $\Delta B_{pu}^{n=1}$ is measured by an array of 12 poloidal field sensors above the device midplane. The amplitude modulation shown in Figure 2.3.2-4(d) is attributed to the interaction of the mode and eddy current fields, and the field generated by the RWM control coils is subtracted from $\Delta B_{pu}^{n=1}$. The $\Delta B_{pu}^{n=1}$ is larger in the non-stabilized plasma as the $n = 1$ RWM becomes unstable, and in the stabilized plasma is controlled at an average level of about 5 G. During $n = 1$ stabilization, the $n = 2$ RWM does not become unstable, although $\Delta B_{pu}^{n=2}$ becomes larger than $\Delta B_{pu}^{n=1}$ at the lowest values of ω_ϕ and highest values of β_N (Figure 2.3.2-4(e)). The actively stabilized, low ω_ϕ plasmas can suffer partial β_N collapse due to largely internal modes, which do not disrupt I_p, allowing β_N to recover. An example is shown by the dotted curves in Figure 2.3.2-4 (a) & (b). DCON stability calculations show that $\beta_N > \beta_{N\,(n=2,\,no\text{-}wall)}$ and are consistent with the identification of this mode as an $n = 2$ internal MHD instability.

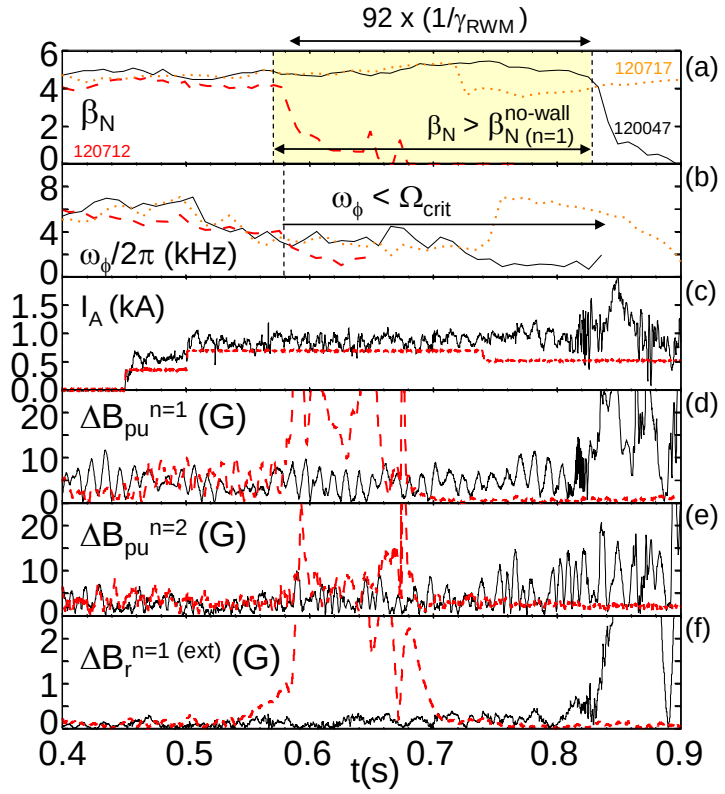

Figure 2.3.2-4 RWM active feedback stabilization in low rotation plasmas. Solid curves: actively stabilized plasma at ω_ϕ significantly below Ω_{crit}, dashed curves: RWM unstable plasma at $\omega_\phi/\Omega_{crit} = 1$ with active feedback turned off, dotted curves: (upper two frames) actively stabilized plasma suffering a beta collapse from an internal $n = 2$ plasma mode. Shown are the evolution of (a) β_N, (b) ω_ϕ near $q = 2$, (c) current in representative non-axisymmetric control coil, (d) and (e) mode amplitude of $n = 1$ and 2 field components measured by the upper B_p sensor array, and (f) mode amplitude of $n = 1$ field component at the midplane, external to the vacuum vessel.

The measured $n = 1$ and 2 RWM amplitude and phase, along with chord integrated soft X-ray (SXR) measurements spanning from the plasma core to the edge [30] are shown in Figure 2.3.2-5. Without active control, the $n = 1$ RWM becomes unstable. At early times in the figure, $\phi_{Bpu}^{n=1}$ appears to wobble between 150 and 300 degrees, eventually settling to the lower end of this range, and as $\Delta B_{pu}^{n=1}$ grows exponentially, $\phi_{Bpu}^{n=1}$ shows mode rotation in the direction of plasma rotation, as expected by theory.

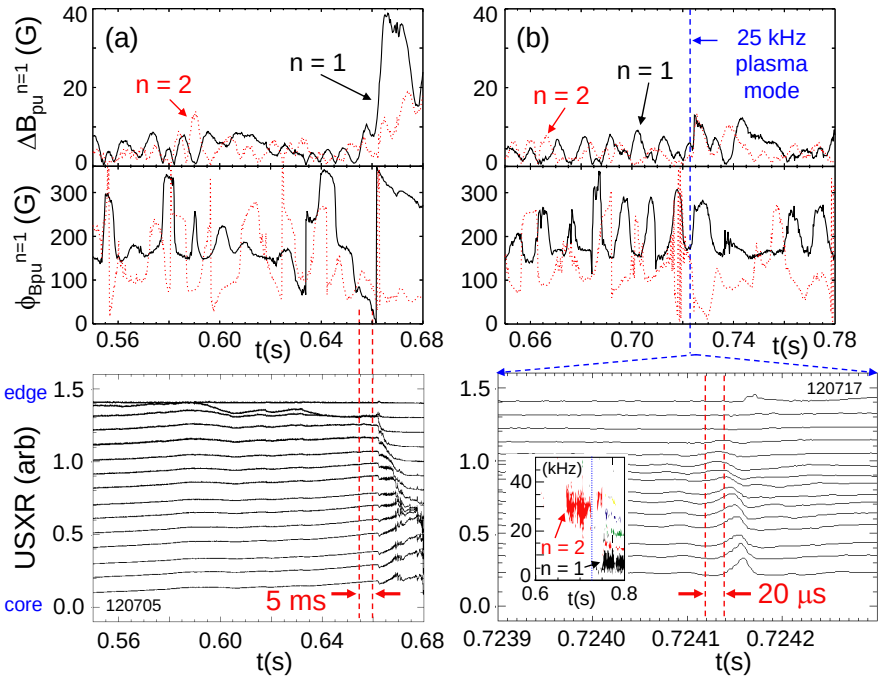

Figure 2.3.2-5 Mode activity in plasmas with and without active stabilization. Frames from top down show upper B_p sensor amplitude, phase, and ultra-soft X-ray emission spanning from the plasma core to edge vs. time. Solid lines: n = 1, dotted: n = 2. Column (a) discharge with active feedback off, column (b) RWM actively stabilized plasma with internal n = 2 plasma mode. Lower frame inset: n spectrum from midplane toroidal magnetic pickup coil array.

SXR data shows the mode amplitude largest in the outer region of the plasma, propagating toward the core during mode growth. The n = 2 RWM amplitude shows periods when $\Delta B_{pu}^{n=2} > \Delta B_{pu}^{n=1}$, but the n = 2 mode growth that eventually occurs, although strong, is subsidiary to n = 1 mode growth. Figure 2.3.2-5(b) shows analogous detail for the actively stabilized plasma suffering a largely internal mode shown in Figure 2.3.2-4. Both n = 1 and 2 RWM activity are stable, with $\phi_{Bpu}^{n=1,2}$ wobbling within some range. SXR data shows mode growth on an ideal MHD timescale, much faster than τ_w, is largely internal, and the measured 25 kHz frequency indicates that the mode is n = 2, since it appears in a region of the plasma with $\omega_\phi/2\pi \sim 12$ - 15 kHz. The n spectrum measured by a toroidal array of magnetic pickup loops also shows n = 2 mode activity at this frequency and time.

RWM stabilization can fail due to a change in the poloidal form of the mode. An example is shown in Figure 2.3.2-6, where the $n = 1$ components of both upper and lower B_p and B_r sensors, and $\Delta B_{r\text{-}ext}^{n=1}$ sensor signals are shown. Note that since the latter sensor is outside the vacuum vessel, the signal lags those of the internal sensors by ~ O(τ_w) ~ 6 ms for $n = 1$. Approaching the time of β_N collapse, $\Delta B_{pu}^{n=1}$ and $\Delta B_{pl}^{n=1}$ first decrease to near zero, as the radial field sensors increase by a small amount. Then, $\Delta B_{pu}^{n=1}$ increases strongly, while $\Delta B_{pl}^{n=1}$ lags, and the ratio $\Delta B_{pl}^{n=1}/\Delta B_{pu}^{n=1}$ never gets above 0.5. There is also a strong increase in $\Delta B_{r\text{-}ext}^{n=1}$ while $\Delta B_{ru}^{n=1}$ and $\Delta B_{rl}^{n=1}$ decrease, indicating that the mode is bulging through the midplane gap in the stabilizing plates and decreasing in amplitude in front of the plates. This observation may indicate a lack of "mode rigidity", normally assumed theoretically and observed experimentally [31].

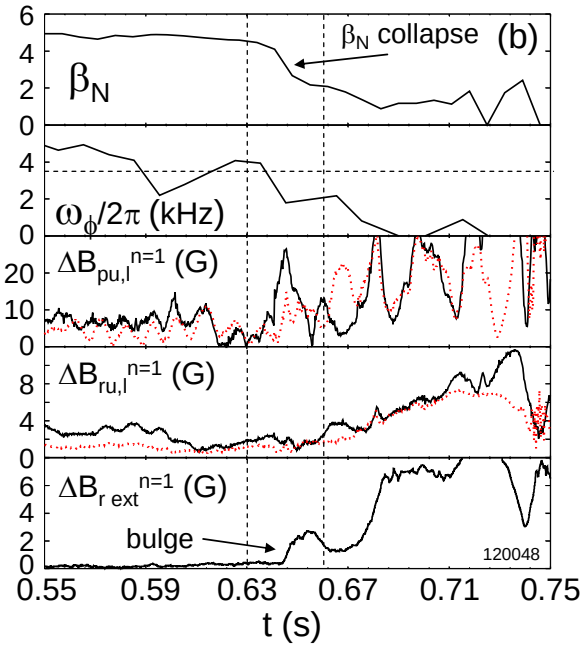

Figure 2.3.2-6 Poloidal deformation and mode destabilization during RWM active stabilization. Sensors are distinguished by solid (upper sensors) and dotted (lower sensors) lines.

This poloidal deformation appears to occur when large RWM coil currents are requested and sometimes when the central q is near unity. These conditions may lead to nearby stable $n = 1$ MHD modes becoming important in the mode dynamics, causing the RWM eigenfunction to apparently change poloidal

structure. The hypothesis of other weakly damped eigenfunctions causing the deformation in this way requires further study. Initial analysis of reconstructed equilibria shows the ideal energy functional for the *second* least stable $n = 1$ eigenfunction becoming sufficiently small for the mode to enter the dynamics when β_N exceeds ~ 5.5. The RWM stability code NMA [32] (Normal Mode Analysis) allows up-down symmetric, 2-D calculations that include more than a single rigid mode and is presently being tested against experimental results from DIII-D and NSTX. The VALEN code has been upgraded to include multiple modes in 3-D geometry and is presently being tested on NSTX, DIII-D, and HBT-EP equilibria.

In experiments through 2008, RWM active stabilization research continued by examining stabilization using a greater array of RWM sensors in the feedback loop (2006 experiments used $\Delta B_{pu}^{n=1}$; 2007-2008 experiments added different combinations of $\Delta B_{pl}^{n=1}$, $\Delta B_{ru}^{n=1}$ and $\Delta B_{rl}^{n=1}$ for feedback.). Development of the active $n = 1$ control system has reached the point where non-RWM experiments are now using it as a routine tool to control RWMs and for dynamic error field correction. More that 10 experiments have used the system in 2008, with more than 200 shots taken so far with $n = 1$ feedback control on. The system is widely used in the 2008 run campaign because unstable RWMs have been observed at intermediate levels of rotation, showing that stability at low plasma rotation does not insure stability at higher rotation. This result contradicts simple threshold models of RWM "critical rotation", and will be considered in the next section sub-section on passive stabilization physics. Discharges at intermediate plasma rotation with and without active $n = 1$ feedback and $n = 3$ DC error field correction (see section 2.3.3 for $n = 3$ correction) are compared in Figure 2.3.2-7. Analysis of the present data will lead to further optimization of the present feedback system in the near term, with focus on mode dynamics during stabilization.

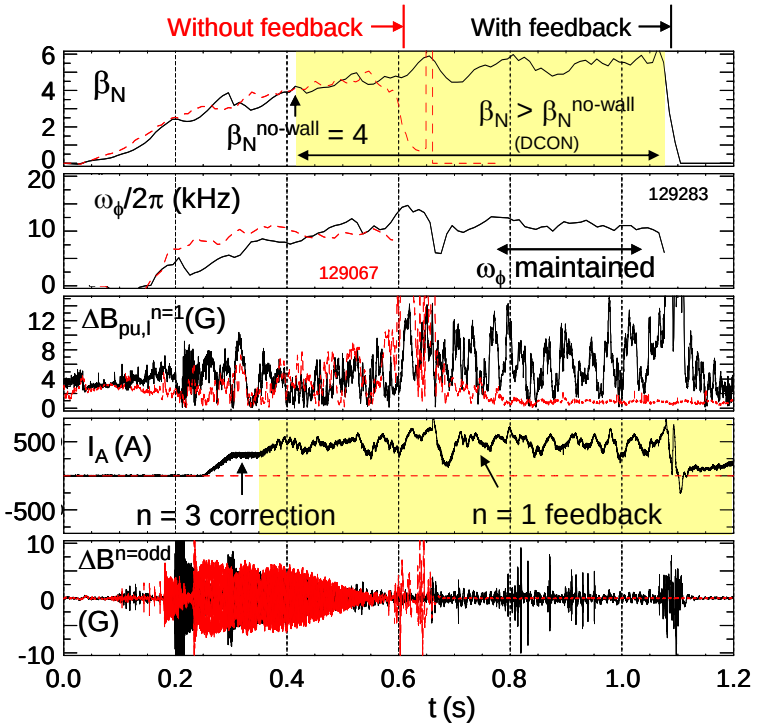

Figure 2.3.2-7: Comparison of discharge encountering RWM instability at intermediate plasma rotation, leading to disruption without n = 1 active feedback and n = 3 DC error field correction (red dashed lines) vs. mode control and resulting long pulse length when RWM control and error field correction are enabled.

(i) physics and control – upgrades and plans

Expanded machine capability in several areas will aid in the RWM research task, and will allow advanced experimentation and comparison to theory. The new capabilities will also expand the applicability of the research to future devices including ITER. The key capabilities planned in the 2009-2013 timeframe are:

(i) Implementation of an additional non-axisymmetric control coil set (NCC)
(ii) Alteration of stabilizing plate material and electrical connections
(iii) Non-magnetic detection of resistive wall mode using soft X-rays
(iv) Measurement of scrape-off layer currents
(v) Advanced active feedback stabilization control algorithms

These capabilities are discussed below in the context of the appropriate RWM stabilization physics to be explored. A timeline summary of the proposed research will complete this section.

Addition of new non-axisymmetric control coil set

In the 2009 – 2013 period, a new non-axisymmetric control coil (NCC) set is proposed (with incremental funding) to serve research functions synergistically across topical groups including RWM stabilization, ELM mitigation, and plasma rotation control. Each research area is covered in this document, with the first and last covered in this MHD chapter, and ELM mitigation via resonant magnetic perturbations discussed in Chapter 5.

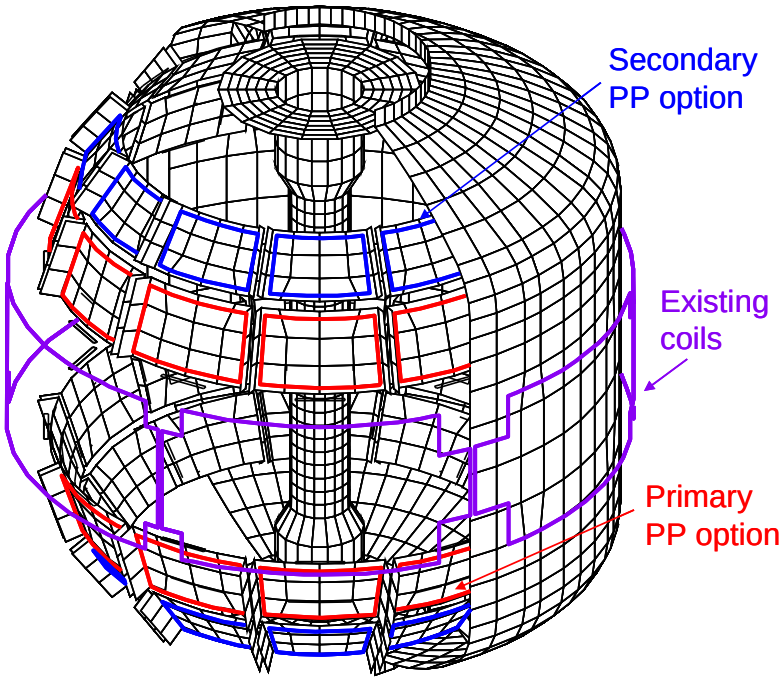

Figure 2.3.2-8 Initial configurations considered for supplemental RWM stabilization coils, which will also be used for ELM mitigation, and plasma rotation control research in the 2009 – 2013 time frame.

The physics design for optimal NCC configurations is presently underway. All research considerations are being considered in this joint design effort, and at present it is agreed that an off-midplane coil set that

is internal to the machine vacuum vessel is desired for all roles. Here, we consider an initial physics design study for RWM stabilization using the VALEN code, analogous to the study performed for the existing RWM stabilization coil on NSTX [10], but with just two simple, non-optimized coil configurations (illustrated in Figure 2.3.2-8).

The present designs consider a total of 24 coils, with two sets of 12 coils each located above and below the device midplane. The large number of coils is primarily desirable for greater n spectrum generation for ELM mitigation and plasma rotation control, but could also be used for future $n > 1$ RWM stabilization. There is ample free space in the vessel in the region behind the primary and secondary passive plates to consider several variations for coil optimization. At present, we consider the following variations: (i) coils behind the primary passive plates and separately (ii) coils behind the secondary passive plates. These coil options have significant overlap with KSTAR and the present ITER VAC02 coil design, and directly support present KSTAR and ITER RWM stabilization and rotation control design efforts by the U.S. In the initial NSTX configurations, the coils are chosen to be parallel to the plates, which is not necessarily an optimal orientation. In the VALEN studies, we also consider changing the present copper passive plate material to stainless steel. The performance of these two coil options are shown in Figure 3.3.2-9 (a) for the present copper passive plate material, and Figure 3.3.2-9(b) for modified stainless steel plate options, displaying mode growth rate at near optimal active stabilization using simple proportional gain. Also shown on the plots are the growth rate curves for the present midplane coil RWM stabilization system on NSTX, passive stabilization growth rate curves, and the with-wall beta limit. The results show that the initial coil geometries chosen in this study should improve control performance only if more resistive plate material such as stainless steel is used. Please note that these are initial, unoptimized coils and plate configurations. Further designs are now being considered to improve control system performance, with the goal of reaching operation at β_N up to the ideal no-wall limit.

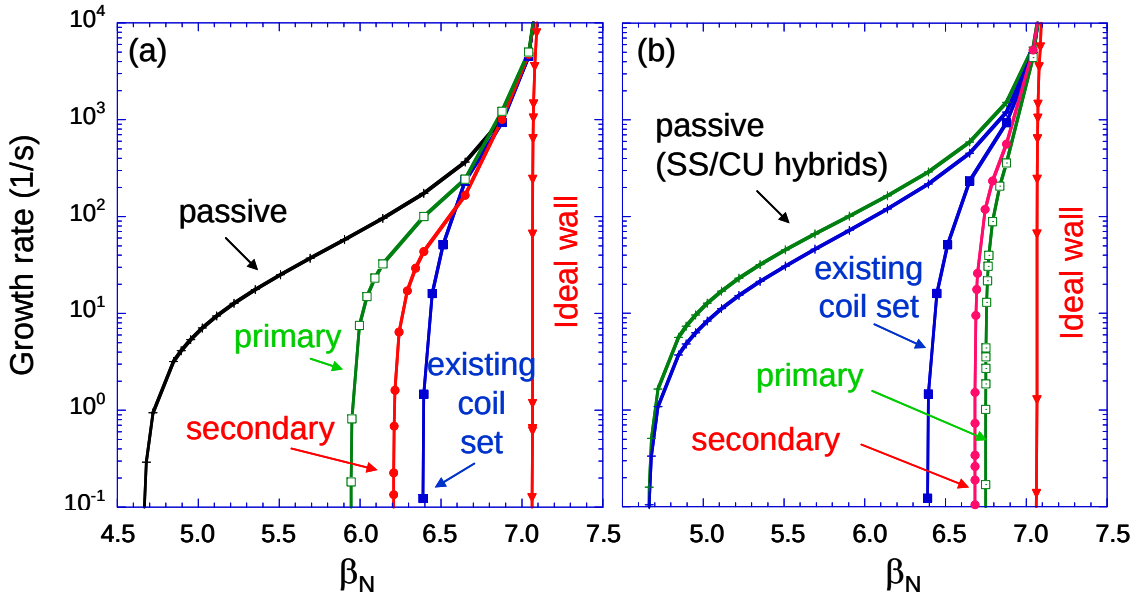

Figure 2.3.2-9 Active RWM stabilization performance of NCC system coil options, (a) for the present copper passive plate material, and (b) for modified stainless steel plate options. Also shown is the growth rate curve for the present external midplane RWM stabilization coil, and the with-wall β_N limit curve. The two passive curves in frame (b) correspond to two possible combinations of primary/secondary passive plates made of copper/stainless steel.

In addition to the increased ability for the internal NCC (behind stainless passive plates) to stabilize the NSTX plasma at higher β_N than the present external RWM stabilization coil, the NCC will allow stabilization of the RWM above/below the plasma midplane, independent of the present external coil at the midplane. Also, if funding is sufficient to allow power supplies to independently power the upper and lower NCC arrays, the stabilization system could be set up to independently respond to the RWM amplitude measured in the upper/lower/midplane $n = 1$ sensors. This configuration would allow a complete study of RWMs displaying poloidal deformation.

The NCC would also allow experiments that would support the use of similar coils for RWM control in ITER. The recent VAC02 coil design for ITER, shown in Figure 2.3.2-10, resembles the coil geometry considered for the NCC, with three rows of toroidal coils, each partially shielded from the plasma by conducting structure (analogous to the ITER blanket modules). VALEN code calculations show that a

substantial increase in β_N is possible in ITER Scenario 4 using this coil (β_N up to 3.8 with active control vs. 2.5 without). Research on the impact and solution of mode deformation and the effect of shielding conducting structure on RWM feedback system performance would prepare for operation of this ITER coil system for RWM stabilization.

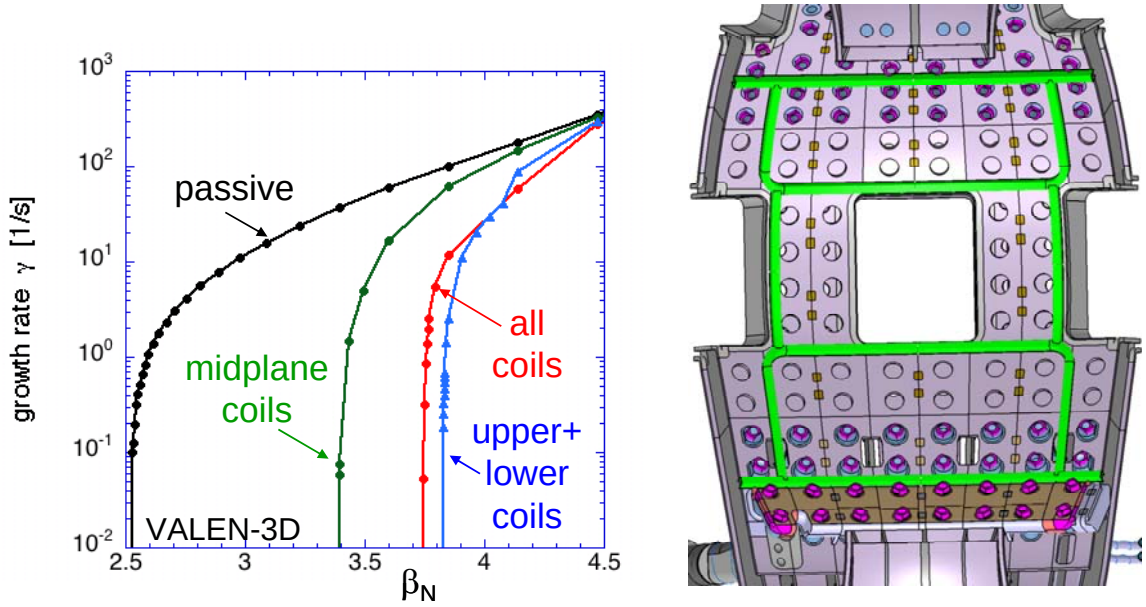

Figure 2.3.2-10 ITER VAC02 non-axisymmetric coil design (40 degree toroidal sector) and computed stabilization system performance.

Alteration of stabilizing plate material and electrical connections

As shown in the active stabilization performance diagrams computed using VALEN, changing the passive plate material from copper to stainless steel in front of the planned coil positions increases the active feedback performance. In addition to this potential change, the VALEN code will be used to determine the optimal way to electrically connect the passive plates. Conceptual design studies conducted before NSTX was built showed that the originally planned $n = 1$ configuration of electrical jumpers led to a substantial error field during plasma start-up. The present lack of connections leads to an $n = 12$ configuration. While eddy currents with an $n = 1$ pattern can be set up in this configuration, it is possible

that an $n = 6$ jumper configuration could yield superior passive stabilization performance. Such configurations will be considered in the NCC design.

Non-magnetic detection of resistive wall mode using soft X-rays

While magnetic sensors are a simple and logical choice for RWM detection and have been used exclusively in RWM feedback stabilization systems in tokamak and RFPs to date [33,34,35], they have several disadvantages. Magnetic pickup from sources other than the RWM sought to be stabilized needs to be subtracted from the measured signals in real-time. While in many cases this can be done for known sources, such as the applied control field, it is difficult or impossible to eliminate all non-desirable field sources by subtraction or filtering techniques (e.g. fields due to currents in significant conducting structures, such as the passive stabilizing plates). Eliminating non-RWM coherent mode activity in the RWM frequency range (e.g. ELMs) is an active area of research [36]. Additional significant issues arise in long pulse burning plasma devices such as ITER or CTF, where long-pulse operation combined with the presence of the electrically-conducting thick metallic blankets and a strong radiation field will make control with conventional magnetic sensors difficult.

NSTX provides an excellent laboratory to research and implement non-magnetic detection of the RWM, partially because such research would serve an immediate practical purpose to both understand and eliminate unwanted field sources due to uncompensated currents picked up by the present magnetic detection system. A possible indication of unmeasured fields in RWM detection in NSTX is the observed amplitude modulation observed in the poloidal field RWM sensors during RFA or RWM activity, which may be caused by the superposition of weakly damped stable RWMs, or unmeasured currents in the closely coupled passive conducting plates or scrape-off layer. The amplitude modulation observed in the present magnetic sensors during stable RWM/RFA activity (Figure 2.3.2-4(d)) appears to be supported by the present multi-energy soft X-ray (ME-SXR) sensor data from the same plasma discharge (Figure 2.3.2-11). As shown in Figure 2.3.2-11a) during the RWM evolution both the poloidal field perturbation amplitude and the high energy ($E > 2$ keV) peripheral SXR signals exhibit an oscillation with ≈ 100 Hz characteristic frequency, showing that there is a plasma component in the frequency range of the magnetic signal modulation. Spatially inverted SXR data in Figure 2.3.2-11b) shows that this oscillation occurs near the plasma boundary, around $R_{tan} \approx 1.45$m.

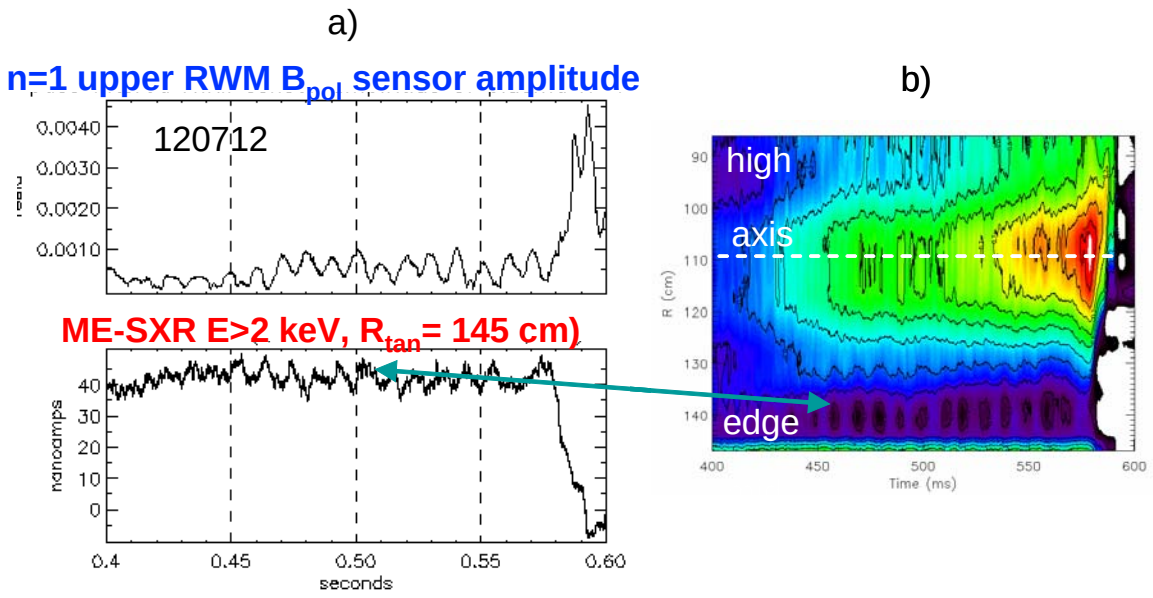

Figure 2.3.2-11 a) Comparison between time history of *n* = 1 RWM Bp sensor amplitude and that of high energy ME-SXR emission from the NSTX pedestal, b) Intensity contour plots of Abel inverted SXR emissivity at high energy.

A dedicated set of ME-SXR sensors will be designed and implemented in the 2009 – 2013 period to both compare magnetic and non-magnetic RWM detection techniques and would be an option for input to the RWM active control system. The ME-SXR system used for RWM detection will comprise a dedicated set of sensors arranged toroidally to best discriminate n = 1 (and perhaps n = 2) mode activity. The system will aim at detecting with high sensitivity and accuracy the RWM toroidal T_e perturbation of the boundary plasma. 'Gradient' ME-SXR sensors, measuring the sharpness of the H-mode pedestal could also be deployed in order to facilitate discrimination between the RWM and the ELM perturbations. The ME-SXR technique is already used as part of the general SXR detection system on NSTX developed by the Johns-Hopkins University collaboration. In addition to the advantages over magnetic sensors mentioned above, ME-SXR sensors also potentially offer much larger signal-to-noise ratio.

Measurement of scrape-off layer currents

The behavior of scrape-off layer currents (SOLC) may be an important component for understanding the diagnosis and behavior of RWMs, as well as ELMs and edge magnetic islands. With measurement of the SOLC, their importance can be evaluated. The potential modification of these currents during use of the present midplane RWM control system and/or with the proposed NCC set can determine how the SOLC affects finite-n feedback. The SOLC flows along an open field lines that terminate at the surface of divertor plates and other structural elements in tokamaks. The return current of a SOLC circuit may flow along another open field line and/or through vacuum vessel wall and other structures. The SOLC has been observed during MHD activity, including ELMs on DIII-D. [37] However, the efficacy of a non-axisymmetric SOLC in creating a non-axisymmetric field, and hence also the question of whether or not the SOLC can play a causal role in the MHD stability, depend importantly on the SOLC's spatial structure, both toroidal and radial. During the 2009-2013 period, NSTX will be outfitted to measure the SOLC using tile current sensor arrays and upgraded Langmuir probe arrays (more detail is given in Section 2.3.6). If found to be important, the VALEN, IPEC, (see Section 2.3.3) and M3D codes can be used to model the effects of the SOLC on RWM stability, dynamic error field amplification or screening, and ELMs.

The version of M3D developed for ELM studies has the capability to extend the usual M3D equilibrium from a closed flux surface out beyond the separatrix and to a possibly resistive wall, treating the vacuum region as a low-density, highly resistive plasma. By imposing a moderate-*m* helical current perturbation in the SOL in this region, supported by a matching source term, the effects of SOLC on the stability properties of MHD modes can be studied. With sufficient measurement and modeling of the SOLC, an investigation can be made as to whether the SOLC could be controlled to suppress or mitigate plasma instabilities. This investigation naturally couples to NSTX experience with RWM control and stabilization physics. If the SOLC can be controlled in ways beneficial to the RWM and/or other low frequency MHD modes, it might allow advantages to present mode stabilization with magnetic coils in future devices with high neutron fluence.

Advanced active feedback stabilization control algorithms

The present RWM active stabilization system on NSTX utilizes simple proportional gain. The physics design of the present stabilization hardware and control system software shows a maximum capability of stabilization up to 74% of the ideal with-wall stability limit [10]. The theoretical inability to reach higher stable β_N is due to the control coil being outside of the vacuum vessel. The geometry is similar to either the baseline EFCC coils or newly proposed RWM control coils in ITER, which will be shielded to various extent by the blanket modules. However, with more advanced software control algorithms, greater stabilization capability in ITER, and in general, is possible [38]. Evaluation of such algorithms has essential importance for RWM stabilization in ITER, as such control algorithms are being considered in the ITER design, yet they have not yet been tested and evaluated in present active RWM stabilization experiments.

Evaluation of algorithms such as the LQG controller [38] is presently underway on NSTX using existing active RWM stabilization data. In the 2009-2013 period, an advanced algorithm for RWM stabilization will be implemented on NSTX to determine the performance of the algorithm compared to simple proportional gain. This research will provide the required experimental verification of advanced algorithms for future devices such as ITER.

Additional potential applications of new capabilities to RWM physics research

The observation of $n > 1$ RWMs during passive stabilization in NSTX, $n = 2$ internal kink modes during $n = 1$ RWM active stabilization, and the ability to violate the $n = 2$ ideal no-wall beta limit indicate that the $n = 2$ RWM may be driven unstable at higher β_N than has been actively stabilized at present. If this occurs during the next 5 year research period, perhaps in conjunction with the addition of the second neutral beam, the NCC set could be configured to stabilize the $n = 2$ RWM while the present external RWM coil is used to stabilize the $n = 1$ RWM. VALEN would be used to determine the capability of stabilizing the $n = 2$ RWM with the NCC. M3D can be used to model the presently observed n = 2 internal link during RWM stabilization. Plasmas with stabilized $n = 1$ RWMs can be modeled by generating suitable stable equilibria with ideal wall boundary conditions as an approximation to $n = 1$ stabilization. A small n=2

perturbation can then be added to the poloidal flow field in the presence of an arbitrary toroidal rotation profile, following which M3D will be run in its linear mode to find unstable eigenmodes, if any, and their growth rates.

The soft X-ray system upgrade is being proposed to have complete poloidal coverage at two toroidal positions. This upgrade will restore prior SXR diagnostic capability that was used to clearly distinguish the $n = 1$ RWM from $n = 0$ perturbations [22], and to expand that capability to greater plasma coverage. Additionally, the use of ME-SXR arrays will enable a direct measurement of the toroidal and poloidal displacement of T_e iso-surfaces.

2.3.2.2 Passive stabilization physics

While passive stabilization has been established with great effect in NSTX (Figure 2.2.1-2) [22], and even simple models of the RWM go far in describing RWM dynamics in general [39], a full understanding of the stabilization mechanism, first-principles or otherwise, remains elusive. Attaining this understanding is a critical milestone in RWM research, particularly for the purpose of confident extrapolation to future devices.

The rotation at the $q = 2$ surface has been used for the past decade as a key parameter to define the critical plasma rotation, Ω_{crit}, required for passive RWM stabilization. RWM research in NSTX has questioned this hypothesis of a scalar critical rotation value for several years [9], and showed success in defining a critical rotation *profile* $\Omega_{crit}/\omega_A = 1(4q^2)$based on analytic theory by Bondeson and Chu [22] (Figure 2.3.2-12(a)). Subsequently, $n = 3$ non-resonant magnetic braking was used on NSTX to reduce the plasma rotation to zero on low-order rational surfaces with $q > 2$ to show that rotation on these surfaces was not required for stability [24] (Figure 2.3.2-12(b)). This result appeared to contradict conclusions made based on DIII-D research highlighting the importance of plasma rotation on outer flux surfaces.

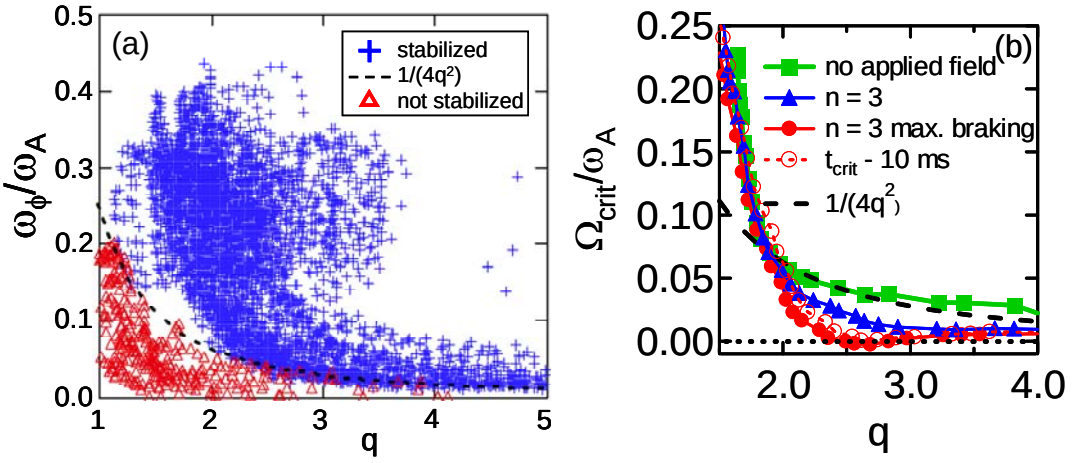

Figure 2.3.2-12 Observed kink/RWM stability vs. local ω_ϕ/ω_A, parameterized by local q value (no applied fields - frame (a)), and variation of marginally stable profile shape using applied non-resonant n = 3 magnetic braking (frame (b)).

Recent results using balanced NBI in DIII-D further call into question the concept of a scalar critical rotation frequency for RWM stabilization [40]. The importance of the Alfven frequency in describing the stability criteria is also called into question, as extremely low values ~ 0.3% are quoted for stabilization at the q = 2 surface. The large difference in Alfven frequencies, due to the large difference in toroidal field magnitude between NSTX and DIII-D, may help to distinguish the important plasma parameters and underlying physics for RWM passive stabilization by conducting further joint experiments aimed at this topic. If, for example, the Alfven frequency normalization is eliminated, the "critical rotation" for RWM stabilization would be comparable in NSTX and DIII-D, indicating that physics leading to this normalization may not be important. Also it has been noted that ion Landau damping is greatly reduced when toroidicity is included in the calculation [41]. This was a key motivation to examine the role of toroidal inertia enhancement, as described in Ref. 41, for RWM stabilization in NSTX [22].

The effect of resonant n = 1 error fields on past RWM critical rotation experiments in DIII-D has been examined, with the conclusion that application of such fields to slow the plasma rotation may explain the higher previously quoted values of Ω_{crit}/ω_A in DIII-D compared to the far lower values in more recent balanced NBI experiments [42]; this was explained using a model of toroidal torque balance [43] similar

to that used to explain tearing mode locking [44]. This past quoted "critical rotation" explanation in DIII-D does not explain the presently observed RWM critical rotation profile in NSTX where n = 3 non-resonant magnetic braking is used to slow the plasma rotation and alter the profile shape [24]. As shown in Figure 2.3.2-13, NSTX data does not follow the critical rotation criteria based on the equilibrium plasma rotation frequency ω_0 shown in DIII-D, indicated by the dashed line in the figure.

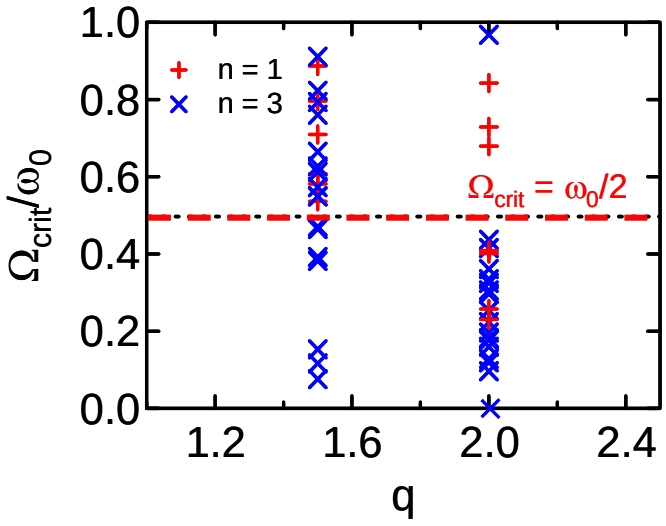

Figure 2.3.2-13 Ω_{crit}/ω_0 at q = 1.5 and 2 showing wide distribution of values with stable discharges down to Ω_{crit}/ω_0 ~ 0.0. The dashed line indicates a proposed critical threshold value for toroidal torque balance to be maintained, which does not apply to NSTX.

Ion collisionality appears to be an important parameter for RWM passive stabilization in NSTX. Shaing's modification of the Fitzpatrick "simple" RWM model [39] includes neoclassical viscosity [45] and introduces a dependence on the ion collisionality to the critical plasma rotation for RWM stabilization. This can be seen by solving for the critical rotation in the high dissipation limit of Shaing's theory, analogous to Equation (26) of Ref. [45], but expanding the solution of the dispersion relation to first order in (γ/μ_1) rather than zeroth order. The result is

$$|\Omega_{crit}| > ((1 - d/d_c)/4 + (1 - d/d_c)^2/\eta^2)^{1/2}, \quad (1)$$

where d is related to the radius of the resistive wall and d_c is related to the maximum radius of wall that will stabilize the external kink mode (the critical wall radius) and $\eta \equiv 1/\mu$, where μ is defined in Equation (24) of Ref. [45]. In the high dissipation limit, the viscous dissipation η scales linearly with ν_i, yielding an inverse dependence of Ω_{crit} on ν_i. Here, ν_i is given by $\nu_i = 4.8x10^{-8} Z^4 m_i^{-1/2} n_i \ln\Lambda T_i^{-3/2}$ sec^{-1}. Therefore, increased ν_i is theoretically stabilizing and yields lower Ω_{crit}. A series of experiments were performed to qualitatively examine the variation in Ω_{crit} with ν_i. The plasma current and toroidal field were scanned together to create a series of discharges with similar shapes, q profiles, and Alfvén speed (v_A), profiles. The density was allowed to vary and a wide variation of ν_i was achieved. Comparing discharges with similar v_A, but varying ν_i indeed shows that increased ion collisionality leads to lower Ω_{crit}. Experiments performed in 2008 using lithium evaporation to change ν_i showed a similar result.

Experiments run through the 2008 campaign show greater complexity of the RWM marginal stability condition and do not support simple models of critical plasma rotation. In particular, intermediate levels of plasma rotation are found to be experimentally unstable, while lower levels of plasma rotation can be stable. Initial results from the kinetic stability model of Hu and Betti [46] show the general behavior required to reproduce experiments. The model contains several resonance effects that modify the ideal fluid energy functional δW. Both rotation and collisionality affect stability by physical processes different than viscous dissipation models in fluid theories. The modified RWM growth rate is expressed as

$$\gamma\tau_w = -\frac{\delta W_\infty + \delta W_K}{\delta W_b + \delta W_K}$$

Where δW_∞ is δW computed with no stabilizing conducting structure, δW_b is computed with a model of the experimental stabilizing conducting structure, and δW_K is the kinetic modification to δW. The effects of trapped ions and electrons, circulating ions, hot particles, and Alfven resonances are included. Examining the modification of δW_K due to trapped ion shows the influence of rotation and collisionality on stability. From Reference [47], Equation 6 we have

$$\delta W_K^{ti} = \int_0^{\Psi_a} d\Psi \left(\frac{p_s}{1+\frac{T_e}{T_i}} \right) \left(2\sqrt{\pi}\frac{r}{\upsilon} \right) \sum_{l=-\infty}^{\infty} \int_{B_0/B_{max}}^{B_0/B_{min}} d\Lambda \left(\frac{\hat{\tau}_b}{2} \right)$$
$$\times \int_0^{\infty} \left[\frac{\omega_{*N} + \left(\hat{\varepsilon} - \frac{3}{2}\right)\omega_{*T} + \omega_E - \omega}{\langle \omega_D \rangle + l\omega_b - i\nu_{\text{eff}} + \omega_E - \omega} \right] \hat{\varepsilon}^{5/2} e^{-\hat{\varepsilon}} d\hat{\varepsilon}$$
$$\times \left| \left\langle \left(2 - 3\frac{\Lambda}{B_0/B} \right) (\kappa \cdot \xi_\perp) - \left(\frac{\Lambda}{B_0/B} \right) (\nabla \cdot \xi_\perp) \right\rangle \right|^2$$

with full definitions found in the reference. The first integration is over flux surface, the second over pitch angle, and the third over particle energy. The integrand of this term shows resonances with the trapped ion precession drift, $<\omega_D>$, bounce frequency, ω_b, the effective ion collisionality, ν_{eff}, and the plasma rotation, which enters the integrand through the ExB frequency ω_E. The integration allows a more complex trajectory through stability space as a function of the rotation profile, which can in NSTX vary from Alfven Mach ~ 0.5 in the plasma core with no magnetic braking, to levels at or below that attained in DIII-D balanced NBI experiments [40] when non-resonant magnetic braking is used.

This model is starting to be tested against the existing RWM marginal equilibrium database for NSTX. As an example, Figure 2.3.2-14 shows contours of normalized RWM growth rate, $\gamma\tau_w$, from the Hu-Betti-Manickam code [47], in terms of the real and imaginary parts of δW_K, using input from an NSTX discharge that becomes unstable at relatively high plasma rotation. Varying plasma rotation from high to low in theory (Frame (a)) shows the plasma move from a region of stability into the unstable region, then return to stability at reduced plasma rotation. This occurs as the different levels of plasma rotation, yielding kinetic resonances of varying strengths (varying energy dissipation). Frame (b) illustrates the dependence of the physics model on ion collisionality, parameterized by variation in Z_{eff}, for another plasma reconstruction. Greater stabilization is found at lower ion collisionality, which is due to the kinetic stabilization effects being more prominent at lower ν_i. This result counters those typically found in simpler fluid viscous models which have increased dissipation at higher collisionality.

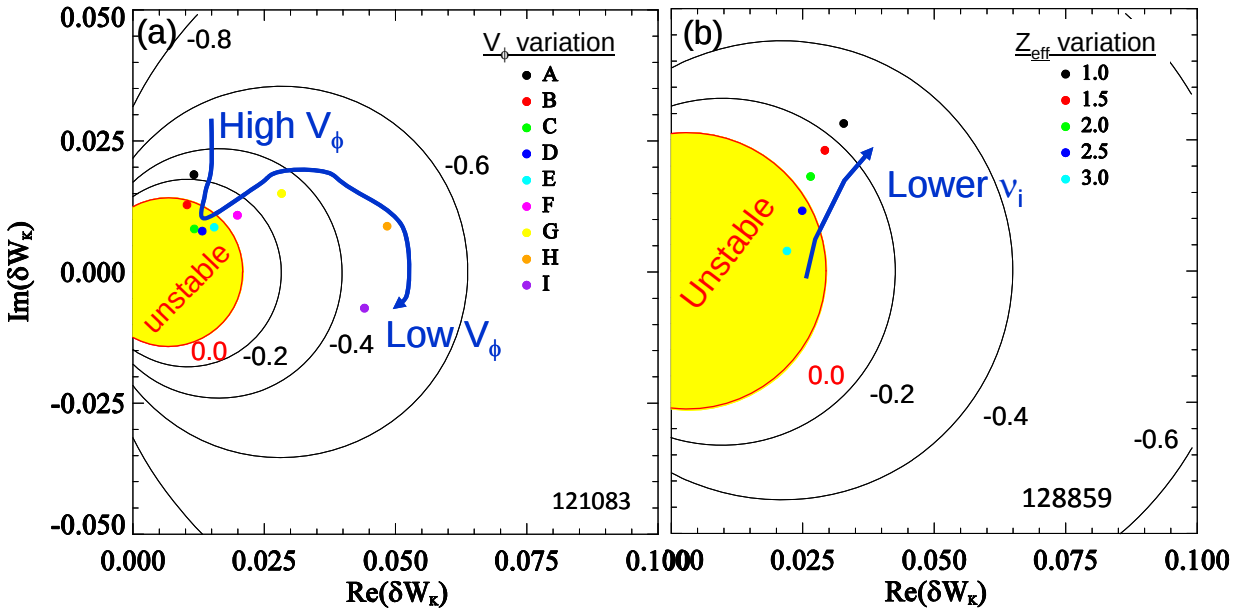

Figure 2.3.2-14: Contours of $\gamma\tau_w$ computed for an NSTX plasma that becomes RWM unstable at an intermediate level of plasma rotation (Frame (a)) and for a plasma used to test stability variation versus ion collisionality (Frame (b)). The measured marginally stable experimental rotation profile best matches the rotation profile variation from fastest (case A) to slowest (case I) at case B or C, in agreement with the computed crossing point into the unstable region.

The kinetic model result is also qualitatively inconsistent with NSTX experiments performed in the past two years, including recent (2008) experiments. These initial results form the basis of further study of the kinetic model to explain RWM marginal stability more generally and to understand the mode stabilization physics. Understanding the physical role of plasma rotation and ion collisionality is key to this study in order to have greater confidence in extrapolations to next-step ST devices. Specific experiments in 2008 will provide further tests, and in the 2009 – 2013 time frame the center stack and rotation control upgrades will go further to both test the physics, and to determine robustly stable rotation profiles to maintain high β_N for long pulse duration.

(ii) physics and control - plans

Planned research to meet the RWM stabilization physics and control goals in the 2009 – 2013 timescale follows two general approaches:

(i) understanding of active stabilization physics and demonstration of reliability at all levels of plasma rotation.
(ii) development and experimental verification of an expanded passive stabilization physics model

Research in the next five years will address key issues to bridge the present gap in both RWM passive and active stabilization physics understanding and system performance. Understanding the role of poloidal mode deformation, $n > 1$ mode activity during $n = 1$ active stabilization, and understanding and implementing improvements to the present active feedback system are important components of RWM active stabilization study. The investigation of using both upper and lower radial and/or poloidal field RWM sensors for mode detection during feedback will continue using the initial experimentation in 2007-2008 to define the next steps. We envision that key physics experiments can be conducted with the present active feedback system for the next few years, and outline several specific upgrades to NSTX capability and diagnostics to take the research into further advanced topics. These upgrade plans and associated studies will be discussed in the balance of this section.

The general plan for RWM passive stabilization research in the 2009-2013 follows from present experimental results from NSTX and DIII-D, but will seek out a new physics paradigm for RWM stabilization that can reproduce the observations of present experiments in NSTX and other tokamaks. One key departure from present theory will be to abandon both the assumption of a single “critical rotation frequency” and most likely the existence of a single critical rotation profile for RWM stabilization. Data to date supports this approach, as new data suggests that the RWM can be destabilized at intermediate to high rotation frequencies, while plasmas with zero rotation at the $q = 2$ surface can remain stable at high β_N. A potential hypothesis that departs least from the existing physics models is one where multiple dissipation mechanisms apply at different levels of rotation and with differing radial localization. The introduction of stabilizing dissipation due to resonance with trapped particle precession

drifts (Hu-Betti theory) may aid in this understanding. Since the kinetic model depends on aspect ratio, ν_i, and rotation profile, NSTX data is important to determine if this physics can be responsible for mode destabilization at high rotation and mode stabilization at low rotation. The new center stack upgrade will expand this study to strongly collisionless plasmas with an order of magnitude lower ν_i. This physics is additionally important to non-ST devices as it should apply to RWM stabilization at plasma rotation levels expected in ITER. Accessing the important range of rotation frequency where trapped particle precession effects become important (similar to the low levels reached in DIII-D balanced NBI experiments) has been demonstrated on NSTX using non-resonant $n = 3$ magnetic braking, and this technique will continued to be used in future studies.

SUMMARIZED RESEARCH PLANS AND TIMELINE

(i) ACTIVE FEEDBACK CONTROL

FY2009-11 Use active RWM feedback as a standard tool for mode stabilization in experiments as desired by session leaders. Continue optimization of the RWM active feedback system at various plasma rotation speeds and profiles by determining the best combinations and relative spatial phase of RWM sensors to be used for feedback, setting of feedback phase (difference between measured mode phase and applied field phase) and other control settings.

FY2009-11 Investigate underlying RWM active control physics, and methods of decreasing the possibility of poloidal deformation of the mode and loss of stabilization. Begin investigation of multiple modes in RWM stabilization and the role of SOLC as additional measurements become available. Determine role of boundary conditions in RWM stability analysis, and the role of plasma response in stabilization using the IPEC code (see section 2.3.3)

FY2009-10 Complete design studies for the proposed NCC, modifications to passive stabilizing structure, and non-magnetic detection of RWMs. Continue analysis of advanced active feedback stabilization control algorithms using present NSTX data and define a

specification for the implementation of these algorithms for RWM feedback control enhancement.

FY2010-13 Implement non-magnetic detection of RWM using soft X-rays, measure RWM activity, and determine how to best process data for future interface to the plasma control system. Determine the role of $n > 1$ RWM activity during $n = 1$ stabilization and expand study when additional NBI power capability becomes available. Examine the role of measured SOLC in stability analysis.

FY2011-13 Implement improvements to passive stabilizing structure and new NCC control coils (incremental). Conduct initial RWM stabilization experiments using the NCC (incremental). Compare stabilization performance with design expectations. Examine the role of $n > 1$ instabilities with second neutral beam. Determine effectiveness of active control in low collisionality plasmas with new center stack.

FY2013 Conduct advanced RWM stabilization experiments using the midplane and new NCC coils (incremental) to produce high reliability of RWM stabilization at the highest β_N possible. Experiments would include prevention of poloidal deformation of mode, $n > 1$ control, high β_N sustainment with active mode control, V_ϕ control, and initial q_0 control.

(ii) PASSIVE STABILIZATION PHYSICS

FY2009-11 Continue research to determine the physics of RWM passive stabilization (a 2009 NSTX milestone) including proposals for joint experimentation with DIII-D. Further examine the role of the rotation profile, Alfven frequency, sound frequency, ion collisionality, applied resonant and non-resonant fields, and kinetic resonances (e.g. trapped particle precession resonance) in RWM passive stabilization.

FY2011-12 Examine passive stabilization in low collisionality plasmas created with the new center stack, and with greater rotation profile variation under V_ϕ control and with new non-resonant magnetic braking torque profile using the NCC. Compare to theory.

FY2012-13 Determine a reliable physics model to confidently predict RWM stabilization as a function of rotation and ion collisionality. Test this model against equilibria created with the second neutral beam (further variation of V_ϕ and q profiles).

2.3.3 Dynamic error field correction

Goal: *Determine sources of dynamically changing error field due to inherent asymmetries in the device and the plasma physics responsible for amplification of these sources. Apply techniques that will dynamically cancel these fields to maintain plasma rotation and stability.*

(i) physics and control - results

Dynamic error field correction (DEFC) involves the detection and correction of non-axisymmetric fields generated during evolution of the plasma discharge. In a low beta plasma, this basically involves correction of static error fields and alteration of those fields based on movement of device components during the discharge evolution. In addition , plasmas of sufficiently high beta will alter these fields, typically amplifying them, while plasma rotation will shield them. The creation of resonant field amplification closely couples DEFC research to RWM research, since RFA is theoretically due to weakly damped (stable) RWMs. [25] At high beta, DEFC is basically the correction of beta-dependent RFA and so is in essence RWM control. A standard distinction between active RWM stabilization or control and DEFC is timescale: “RWM control” is typically used to describe control of unstable modes (up to a few times the RWM inverse growth rate) and “DEFC” is typically used to describe control of stable modes (timescale of changes in β_N, therefore τ_E). When the RWM growth rate is slowed to $O(1/\tau_E)$, the distinction is not clear, nor is highly important. In general, DEFC is critical for reliable, high performance plasma operation, aiming to reduce low beta locked mode density thresholds as well as minimizing drag due to non-axisymmetric fields, maintaining plasma rotation and maximum β_N.

Dynamic error field correction has played a significant role in allowing the highest performance plasmas in NSTX, and the correction of $n > 1$ fields (specifically, $n = 3$) was found to be important. Initially, open-loop correction of the low beta dynamic error field due to movement of components such as the center stack leg of the toroidal field coil was addressed, with good success during the plasma startup through the plasma current flat top. Utilization of the closed-loop $n = 1$ feedback system was subsequently used, providing correction over the full pulse including the high β_N phase of the discharge, yielding the longest pulses and maintenance of plasma rotation.

The method utilized for training the feedback system for n=1 DEFC is illustrated in Fig. 2.3.3-1. A reference discharge with no current in the RWM coils is shown in black; it achieves β_N~4.5, above the no-wall β limits for these class of plasmas. The next case, in red, has a pre-preprogrammed n=1 field, but with the feedback turned of. The applied error field is amplified by the RFA response of the plasma, resulting in increased rotation damping, and an eventual RWM followed by a rotation and β collapse. The two cases in green and blue have the same pre-programmed n=1 error field, but feedback proportional gains of 0.5 and 0.7 respectively. Importantly, the direct coupling of the RWM coils to the in-vessel sensors is removed by the realtime software before the mode decomposition is calculated and the feedback requests generated; the system is thus feeding back on only the measured RFA response. The feedback system produces current requests that attempt to cancel the applied error field, and increasing the gain leads to improved cancellation. The key step is to then to turn off the applied error field, but retain the optimized feedback settings.

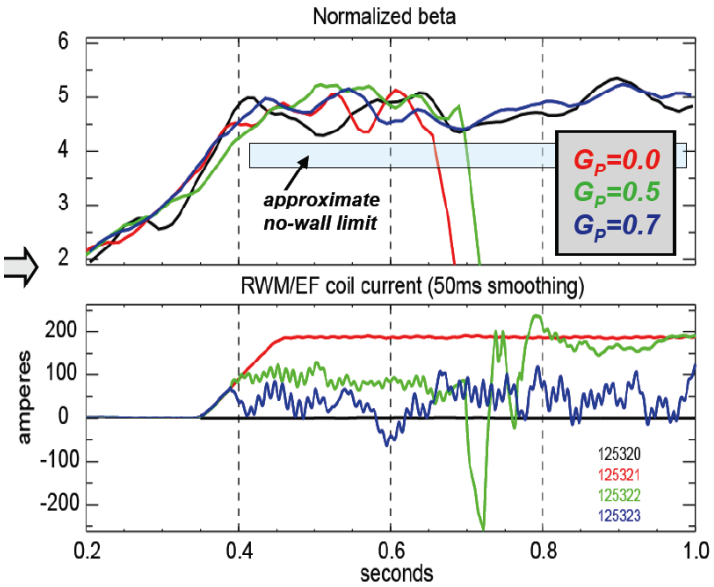

FIG 2.3.3-1: Optimization of the feedback system for dynamic error field correction. The top frame shows the β_N traces while the bottom shows the current in a representative RWM coil. The feedback proportional gain and approximate no-wall limit are shown in the top frame.

In 2007, it was found that discharge pulse length depended on the polarity of an applied n = 3 field, which is typically used for non-resonant magnetic braking (see section 2.3.5). Figures 2.3.3-2 a) and b) show the plasma current and β_N for cases where different levels of n=3 braking, shown if frame c), were applied. There is a clear extension of the high-beta phase and pulse length with n=3 fields of favorable phase. The peak rotation and pulse lengths occur at approximately 300A of n=3 current in the favorable phase. This is significantly lower than the 0.8 – 1.0 kA level of current typically used to control plasma rotation in NSTX by n = 3 magnetic braking.

Further experiments in 2008 have indicated that the required n=3 correction level is likely tied to the PF5 coil current. This is consistent with the measured shape of the coil, which is predicted to produce a predominantly n=3 field. A future upgrade will be to tie this n=3 correction to the PF5 current in the realtime system, allowing more accurate n=3 correction over a range of plasma conditions. In 2008, n = 2 fields were generated using the RWM control coil for the first time in NSTX, and a dedicated experiment was not able to increase plasma rotation, indicating that n = 2 error fields may not be significant.

However, applying the n = 2 fields with only six coils also generated a significant n = 4 component, which may complicate the analysis.

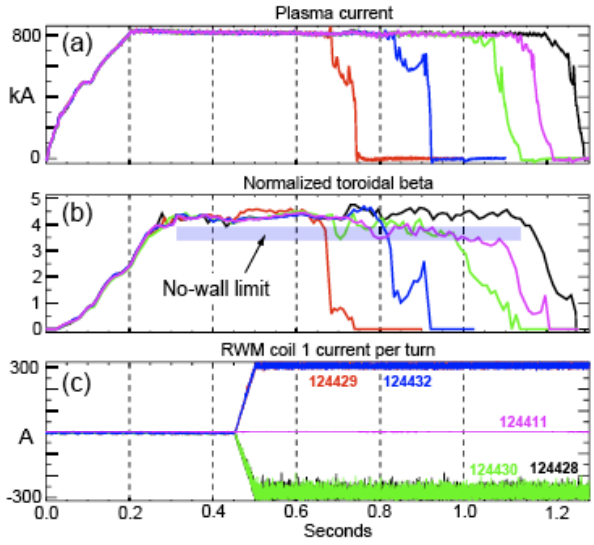

Figure 2.3.3-2 Increased pulse length observed with n = 3 applied field with favorable phase, as evidenced by the pulse length (a) and sustainment of the high-β state (b). The RWM coil current, applying a pure n=3 spectrum, is shown in (c).

These error-field correction techniques have been utilized to develop long pulse discharges with sustained high values of β_N and rotation. An example is shown in Fig 2.3.3-3, where the dynamic error field correction was accomplished by preprogrammed n=3 correction and optimized n=1 feedback based on the combined upper and lower $\Delta B_p^{n=1}$ sensors. This discharge had superior discharge characteristics, including a very long period free of rotating MHD modes and a steady *increase* of the edge rotation, compared to the typical decrease observed without DEFC. Note that this class of discharges has been further improved through the use of lithium conditioning.

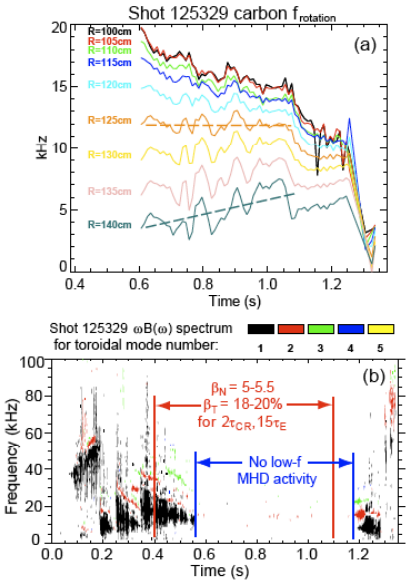

Figure 2.3.3-3 Plasma rotation evolution (top), and MHD activity (bottom), for a long-pulse discharge facilitated by DEFC. This class of discharges has been further improved by lithium conditioning.

These favorable results motivate further study to increase the effectiveness of DEFC in producing plasmas with greater pulse duration, maintaining high β_N and plasma rotation for as long as device limitations (OH flux consumption, coil heating) will allow. Plasmas already produced with pulse durations greater than one second typically allow sufficient time to conduct desired experiments and allow a ramp-down of the plasma current in a controlled manner.

(ii) physics and control - plans

DEFC research is an essential part of bridging the present operation of NSTX to the long-term 5 year goal of demonstrating sustained operation of high confinement, high beta plasmas with high reliability, and so will remain an active area of study in the 2009 – 2013 period. It will remain closely coupled to RWM stabilization research, as the studies and control hardware and software are highly complementary. As high levels of plasma rotation generally appear favorable for both confinement and stability and will likely lead to passive stabilization in future NBI-driven devices such as CTF, understanding the physics regarding the effect of error fields in high beta NSTX plasmas is key to future extrapolations.

Research in this regard will utilize the Ideal Perturbed Equilibrium Code (IPEC), [48] which has been used to evaluate the plasma response to error fields in DIII-D and NSTX, allowing their accurate correction. [49] IPEC finds 3D perturbed scalar pressure equilibria with shielded islands in tokamaks. Given a 2D tokamak equilibrium and an external perturbation, an ideal perturbed equilibrium can be determined by solving the force balance $\vec{\nabla}\delta p = \vec{j}\times\delta\vec{B} + \delta\vec{j}\times\vec{B}$ with boundary conditions set by external coils while preserving the pressure $p(\psi)$ and the safety factor $q(\psi)$ profiles in the plasma. IPEC augments DCON and VACUUM stability codes to solve the force balance given a set of perturbed field $\delta\vec{B}\cdot\vec{n}_b$ on the plasma boundary, and uses virtual surface currents on the boundary to match the set of $\delta\vec{B}\cdot\vec{n}_b$ with a set of externally given field $\delta\vec{B}^x\cdot\vec{n}_b$. The total field $\delta\vec{B}\cdot\vec{n}_b$ and the external field $\delta\vec{B}^x\cdot\vec{n}_b$ are linearly related to $\delta\vec{B}\cdot\vec{n}_b = \hat{P}\,[\delta\vec{B}^x\cdot\vec{n}_b]$ by a permeability operator P on the plasma boundary. The perturbed field and displacement found by IPEC includes the effects by perturbed currents in the plasma (plasma response effects) as well as the externally given field. These effects can substantially change the perturbed field and displacement in tokamak. A comparison of two-dimensional equilibrium flux surfaces for NSTX, and corresponding IPEC perturbed flux surfaces formed by an applied n = 1 field configuration are shown in Fig 2.3.3-4 (a) and (b). It can be seen that the flux surfaces inside the plasma boundary are only deformed in the IPEC equilibrium. Macroscopic stability physics involving ideal flux surface perturbations, such as RWM deformation and correction (Section 2.3.2.1), and associated neoclassical toroidal viscosity causing plasma rotation damping (Section 2.3.5) can be studied using IPEC.

The present form of IPEC has the limitation of not including the currents associated with anisotropic tensor pressures. The tensor pressure IPEC is the next step of the research, which could be completed within a couple of years, will allow a more complete evaluation of shielding currents and may provide greater insight into RWM control by plasma rotation Also, IPEC can be modified to allow islands at one or multiple rational surfaces. An example of such an equilibrium is shown in Fig 2.3.3-4(c), without the plasma response, but the modified IPEC with islands will include the perturbed plasma currents. This relaxed IPEC can allow the study of the interactions of external perturbations with neoclassical tearing modes as another important application.

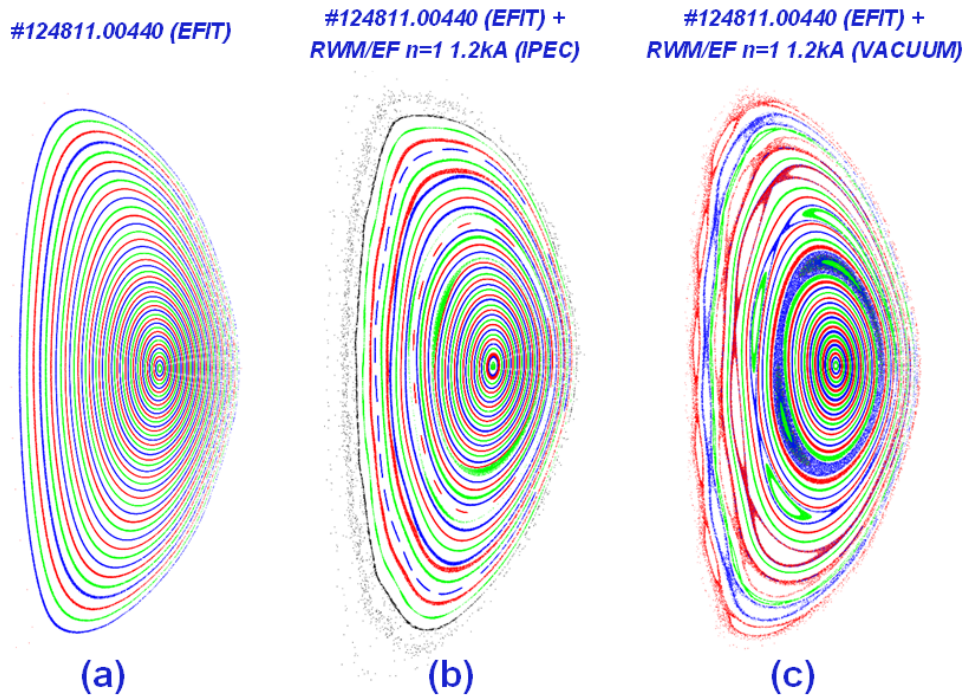

Figure 2.3.3-4 The reconstructed (a) 2D equilibrium, (b) IPEC perturbed equilibrium, and (C) perturbed equilibrium with superposed vacuum field, in NSTX with an n=1 perturbation generated by the midplane non-axisymmetric coils.

DEFC research and practical correction of the field in real-time will benefit from the installation of the upgraded non-axisymmetric control coil (NCC). Simultaneous correction of n = 1, 2 and 3 fields would be possible with significantly improved flexibility in the 2009-2013 period with the NCC. The design of this system for most effective DEFC will be analyzed using IPEC and VALEN. With the coil upgrade and additional power supplies, $n > 1$ fields could be made to toroidally propagate to better match the error field evolution, and the poloidal spectrum of the dynamic error field could be significantly better matched (the present midplane coil does not allow a significant change in the poloidal spectrum of the correcting field). In general, upgrades to the RWM active control system discussed directly transfer for use in DEFC.

SUMMARY OF RESEARCH PLANS AND TIMELINE

FY2009-11 Continue DEFC studies experimentally and with IPEC to further investigate sources of dynamic error field and implementing methods of correction. Develop calculation of tensor pressure equilibria in IPEC. Experimental data will provide field amplification and shielding data as needed to validate IPEC tensor-pressure predictions.

FY2011-12 Evaluate changes to DEFC required to optimize plasmas created with new center stack. Modify IPEC to allow the formation of magnetic islands at one or multiple rational surfaces. Compare to experiments involving the interaction of external magnetic perturbations and tearing modes.

FY2011-13 Utilize the NCC (incremental) to expand the flexibility and capability of DEFC (correction of n number up to 6) to reliably sustained high β_N plasma operation. Develop self-consistent theory of flow-damping by intrinsic error fields and 3D externally applied fields to calculate optimal correction of error fields at high beta. Compare to NSTX experimental data and utilize in real-time error-field control algorithms as applicable.

2.3.4 Tearing mode / NTM physics

Goal: *Study neoclassical and classical tearing modes in the unique low aspect ratio, high beta, and large ion gyro-radius plasmas available in NSTX, in order to both extrapolate our understanding to future ST devices and provide data complementary to that from conventional aspect ratio tokamaks. Investigate the impact of these modes on plasma beta, rotation, fast particle redistribution, and the potential of low aspect ratio operation as being theoretically favorable for NTM stability. Determine scenarios that allow operation without these deleterious instabilities.*

(i) physics – results and plans

The neoclassical tearing mode (NTM) is a magnetic island driven by a hole in the bootstrap current. These modes are a likely problem for any high-performance tokamak, leading to confinement degradation (soft β limit) in the case of the m/n=4/3 and 3/2 modes, and potential mode-locking and disruption for the 2/1 NTM [50]. These modes were studies in early NSTX [51] research, and have been observed in MAST [52]. We plan a renewed focus on NTM physics in the coming research period. Important areas for proposed NTM research include i) investigation of the onset-β and marginal island widths as functions of kinetic parameters and plasma rotation ii) studies of the NTM triggers in q_0>1 regimes, iii), modeling these modes in low-aspect ratio geometry including the effects of flow and flow shear, and iv) studies of the interaction of NTMs with fast particles, including particle redistribution during mode activity.

The degrading effects of an m/n=2/1 NTM on a high performance discharge are shown in Fig 2.3.4-1. The mode amplitude is shown in frame a), with the mode striking at t=0.56 and maintaining it's saturated state until t=0.71, when it locks; the plasma then disrupts at t=0.75. Frames b) and c) show that β_N continually drops during the period of the mode, as does the energy confinement time (both determined by the EFIT code with partial kinetic constraints). The mode has a profound effect on the rotation profile: an immediate collapse of the core rotation and transition to rigid-body rotation. Indeed, it is likely that both the short-circuiting of the magnetic surfaces [53] and the reduction of rotation and rotation shear contribute to the severe confinement degradation. It is clear that in NSTX as well as conventional tokamaks, these modes must be avoided in order to maintain the desired high-β state.

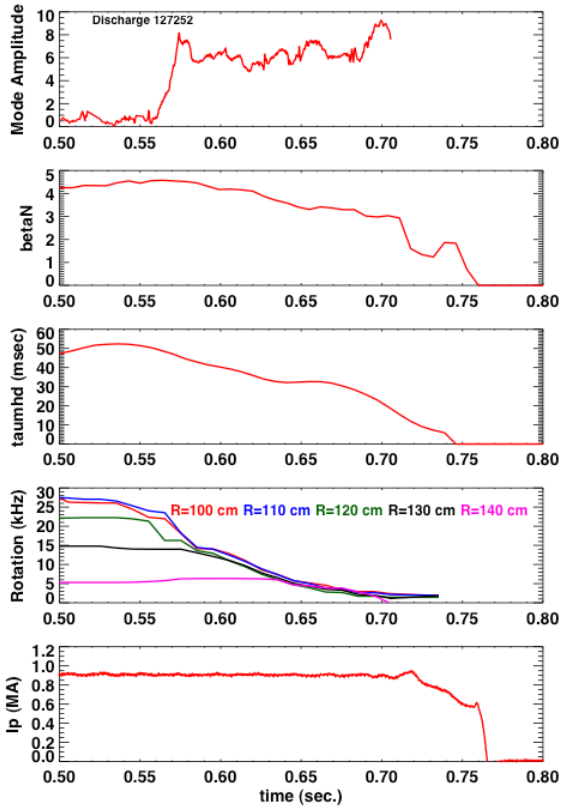

Figure 2.3.4-1: **Illustration of the effects of a 2/1 NTM on discharge confinement. From top to bottom are the mode amplitude, β_N, τ_E, the rotation frequency at five radii, and the plasma current.**

The Modified Rutherford equation (MRE) provides a convenient basic framework to consider for the NTM studies described below:

$$\frac{\tau_R}{r_s}\frac{dw}{dt} = r_s\Delta' - \frac{6r_s D_R w}{w^2 + w_d^2} + \sqrt{\frac{r_s}{R}}\frac{L_q}{L_P}\beta_P r_s\left(\frac{w}{w^2 + w_d^2} - \frac{w_{pol}^2}{w^3}\right) \quad (1)$$

This equation describes the evolution of the full island width (w), including classical tearing stability (Δ'), neoclassical drive due to the bootstrap current missing inside the island ($\propto \beta_P/w$), stabilizing terms due to toroidal geometry ($D_R/w \propto \beta/w$, the "Glasser, Greene and Johnson" term), and threshold effects (the transport threshold manifested by w_d [54] and the polarization threshold manifested through w_{pol} [55]) which are important for small islands. Given that β can begin to approach β_P in NSTX, the GGJ term is expected to be strongly stabilizing [56], an effect to be examined as these studies move forward.

Additional terms can be added to this equation, such as those associated with stabilizing electron cyclotron current drive (ECCD) [57].

Equation 1 predicts that for saturated island sizes larger than w_d and w_{pol}, the island width should be proportional to β_P. This trend is indeed observed, as illustrated in Fig. 2.3.4-2, where the square root of the m/n=2/1 magnetic fluctuation amplitude at the wall ($\propto$ to the island width), is plotted against the global β_P for four discharges where NBI power ramp downs occurred. The linear relationship is clear. This observation, coupled to the close frequency match between the magnetic fluctuations and the q=2 rotation frequencies and the observation of flat spots at q=2 in the electron temperature profile, confirms that the observed mode is indeed a neoclassical island. Similar observations have been made for the 3/2 NTM as well, and the physics discussed above and below is typically relevant to both modes.

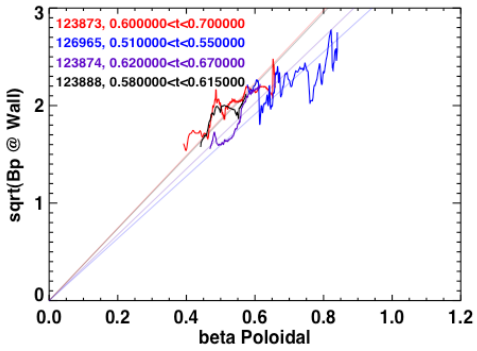

Fig 2.3.4-2: The measured m/n=2/1 island width $\left(\propto \tilde{B}_{P,wall}\right)$ is proportional to β_P, as expected for a saturated NTM.

The small island terms in (1), w_d and w_{pol}, prevent NTM growth for arbitrarily small islands when classical tearing is stable ($\Delta'<0$). Instead, a seed island must be formed whose width exceeds some threshold value. For the 3/2 NTM, this seed-island is typically provided by sawteeth in conventional aspect ratio tokamaks; ELMs have been suggested to play a similar role for the 2/1 NTM in DIII-D and JET. In NSTX, rapid changes in the beam timing have been observed to trigger the 3/2 NTM. The NSTX discharge illustrated in Fig. 2.3.4-3, however, shows a large 2/1 NTM growing with no observable trigger. The spectrogram from a single Mirnov coil in the top frame shows the mode growing at t=0.83, with no precursor; this smooth growth is clearly indicated in the mode amplitude plot in the frame below. Neither

the H_α nor the edge and core USXR signals show a precursor. The NTM eventually locks at t=0.95, as evidenced by the rapid drop of the edge USXR signal and spike in H_α, followed by a disruption. It is possible that cases like these begin as classical tearing modes, which transition to neoclassically driven modes when the island width exceeds the critical island width [58]. This classical physics can be especially important for high-β plasmas, where a pole in Δ' occurs at the ideal kink limit [59]. This discharge had β_N=4.3 when the mode struck, near to if not exceeding the no-wall limit. Understanding this triggering will be an important part of NSTX research.

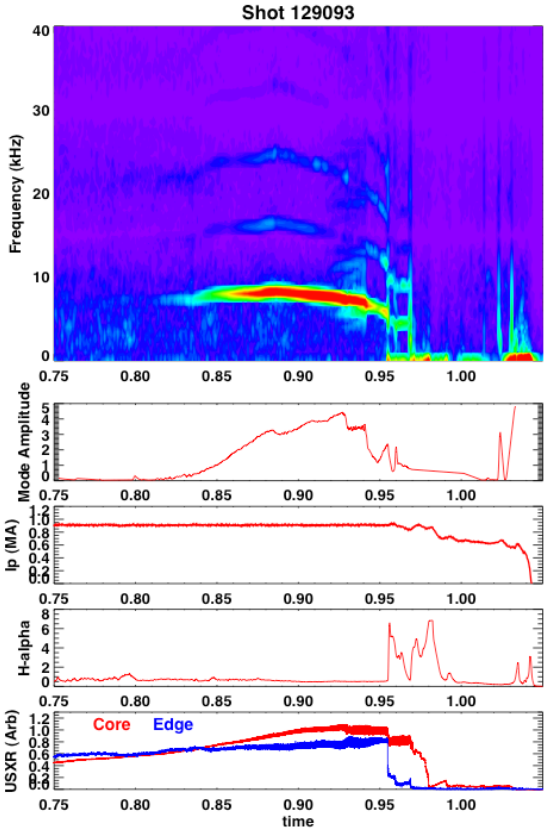

Fig 2.3.4-3: Example of an m/n=2/1 NTM with no clear trigger.

The marginal island width, i.e. the island width where dw/dt=0 for the smallest β_P where NTMs are still metastable, is a key parameter for understanding the relevant small island physics (w_d and w_{pol}) and extrapolating to larger and hotter plasmas. Experiments at conventional aspect ratio in DIII-D [60], JET [61] and ASDEX-U [62] suggest that the marginal island width scales empirically with the poloidal

gyroradius. Verifying this empirical scaling at low aspect ratio is particularly important, as it predicts that an ST reactor or CTF (or indeed, ITER) will be very susceptible to NTM destabilization, and that NTM control techniques must be implemented. β_P ramp down experiments will be conducted to establish the marginal island widths for both the 3/2 and 2/1 NTMs, as a function of parameters such as rotation and poloidal gyroradius. It is planned to make a first complete set of marginal island-width experiments in the FY09-FY11 time-frame. However, the extended field and current capabilities of the upgraded NSTX will expand the parameter regime in quantities like poloidal gyroradius, collisionality, q_{min} and q-shear, providing greater a wider range of applicability for the results.

Plasma rotation and rotation shear enter the eqn. 1 in a number of places, for instance through the polarization threshold term and through modifications to Δ', as well as through mechanisms outside of the MRE, such as modifications to the coupling between the rational surface and the surface where triggering instabilities occur. Given that the momentum input to a future reactor is likely to be much reduced compared to present experiments, there has been recent interest in how rotation and rotation shear experimentally impact the onset and saturation of NTMs. Experiments in JET and DIII-D demonstrated the importance of rotation in increasing the NTM threshold [63]. For the 3/2 NTM, this effect may be associated with dynamic rotation shielding between the NTM resonant surface and the q=1 surface, where the seed perturbation originates. Experiments in DIII-D have also demonstrated a reduction in the onset β for 2/1 modes when the co-injection beam torque is reduced to and beyond zero [64].

Experiments in NSTX have begun to study the dependence of the 2/1 mode onset on rotation shear. We have observed a ~20% reduction in onset global β_N as the rotation at q=2 is reduced. However, given that the NTM evolution in eqn. (1) is determined by local parameters, we have undertaken more systematic studies in terms of local bootstrap drive and rotation shear. Fig. 2.3.4-4 shows the local neoclassical island drive at mode onset, $\mu_0 \langle J \cdot B \rangle L_q \Big/ \sqrt{\langle B_P^2 \rangle}$, where <J·B> is determined for the Sauter model for the bootstrap current, as a function of the normalized rotation shear at q=2, $\left(\frac{d\Omega}{dR}\right)\tau_A L_s$. The discharges in the scan were chosen from a wide variety of experiments which utilized n=3 braking and NBI torque to vary the rotation. All were high-κ, high-δ plasmas with I_P=1MA and B_T=0.45T, typical of

high-performance regimes in NSTX. There is a clear offset-linear dependence of the bootstrap-drive on rotation shear when the mode strikes, implying the importance of rotation shear in allowing higher-β operation. Importantly, this is the first ever correlation of the local NTM properties with local rotation shear, expanding on the previous DIII-D work.

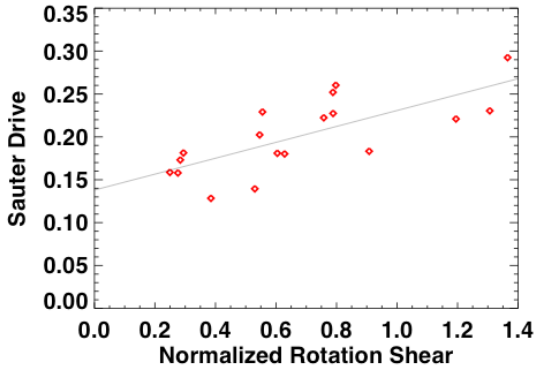

Figure 2.3.4-4 Local bootstrap drive and a function of rotation shear at q=2, for discharges high-κ, high-δ discharge. Both n=3 braking and variations on the NBI are used to vary the rotation shear.

There may, however, be NTM physics outside the direct purview of eqn (1). For instance, the tearing modes in TFTR [65], AUG [66], and possibly other major tokamaks, are commonly coupled to core kink-like modes. As these internal kink-like modes resemble the fishbone instability, it is reasonable to view this as a mechanism through which NTMs are coupled to the fast ion distribution. Evidence for such coupling, e.g., strong frequency chirping, has not been seen as yet in NSTX, though it has been observed in AUG [67] and TFTR. However, NSTX presently operates in a fast ion regime far from typical operating regimes of present large aspect ratio tokamaks. The upgrade to the center stack will allow higher field operation, bringing NSTX fast ion parameters more in line with those of conventional tokamaks. This will allow experiments to study the interactions of fast ions, including potential drive mechanism, with NTMs.

These experimental tasks will be executed in parallel with modeling and simulations of NTM dynamics at low aspect ratio. A three part modeling effort is planned in this regard, involving the linear dispersion relation describing the threshold for onset of the mode, the quasilinear island evolution equation for

intuitive study of the effects of low aspect ratio, and the simulation of mode onset and evolution with initial value codes. The presence of toroidal flow shear introduces a number of physics issues into these analyses, which are critical to understanding the experimental outcome. Experimental discharges that exemplify the physics of flow shear effects on the onset and evolution of these resistive MHD instabilities will be compared to theoretical predictions.

The effect of a sheared flow field on the coupling between modes can be described by the solution to the dispersion relation $\det(D' - D(Q)) = 0$ where D' includes both tearing (Δ') and interchange parities, $D(Q)$ is the solution vector inside of the resonant layer, and Q is the normalized growth rate. With flow shear, Q becomes complex in the sense that the growth rate now has both real and imaginary parts in the inner layer $Q \equiv Q_r + iQ_i$ where $Q_r = k \cdot V_\phi$ (ignoring poloidal precession from ω_* effects) represents the toroidal angular frequency at the rational surface, and Q_i represents the mode growth rate. This directly affects the coupling between modes in toroidal geometry, as addressed at length in [68] and recently published in Ref. [69] as well as the local stability via the inner layer physics, as described in [70], among several others.

In this research plan, we intend to compute the tearing and interchange solutions for multiple rational surfaces using the PEST-III code, and compute the inner layer solutions using the code described in Ref. [71] to solve the dispersion relation. The individual effects can then be examined and compared with a similar approach using the NIMROD code.

A further step will be to implement solutions of the MRE (equation 1) in full low aspect ratio geometry. These studies were begun in the work by [72], where PEST-III was used to calculate Δ', and routines from NIMROD were used to calculate the bootstrap drive and D_R. These steps will allow full calculations of the island growth and decay rates, as well as the saturated island eigenfunctions, for comparison with the experimental measurements described above. A primary goal of these efforts will be to assess the impact of the GGJ term in the context of experimental measurements.

A more advanced modeling step will be to utilize initial value codes such as M3D and NIMROD to simulate the non-linear evolution of NTMs. Compared to the approach in equation (1), these methods are

far more advanced in their treatment of heat conduction around the island, the effects of rotation shear, and self consistent current profile and island width evolution.

A thorough theoretical and computational analysis of the effects that low aspect ratio will have on the resistive stability will be complimentary to the results from the experiment. Also, a comparison with results from the high aspect ratio experiments will give us insight to further develop our theoretical description of the physics of these instabilities.

Our ability to meet these scientific goals will be augmented through improved diagnostic coverage during this research period. NSTX plasmas are overdense, preventing traditional measurements of island widths via electron cyclotron emission (ECE); measurements to date have relied on edge magnetics and USXR emission to constrain the island size and location. However, the BES system currently under construction will allow core fluctuation measurements with high frequency and spatial resolution. The CIF-MSE system also has the ability to measure spatially localized fast magnetic fluctuations at NTM relevant frequencies. This measurement, combined with USXR emission and edge magnetics, should allow detailed studies of the island eigenfunction, including the coupling to internal kink-like modes if present.

(ii) NTM Control

The results in Fig. 2.1.1-1 illustrate that 2/1 NTMs must be avoided in order to maintain optimal performance in NSTX. Experiments in DIII-D, JT-60, and AUG have demonstrated the ability to suppress both the 2/1 and 3/2 NTM with ECCD replacing the missing bootstrap current. This method is not available in the overdense NSTX plasma. Hence, passive control techniques will be employed in the planned research period.

To date, the most successful means of mitigating the 2/1 NTM has been through the use of combined lithium conditioning and dynamic error field correction. This is illustrated in Fig. 2.3.4-5, where the mode activity is compared between discharges with and without lithium evaporation; the rotation frequency in the core and at q=2 are also shown, based on CHERS data and equilibrium reconstruction. Both discharges show a period of MHD activity during and immediately after the current ramp, as the q-profile evolves.

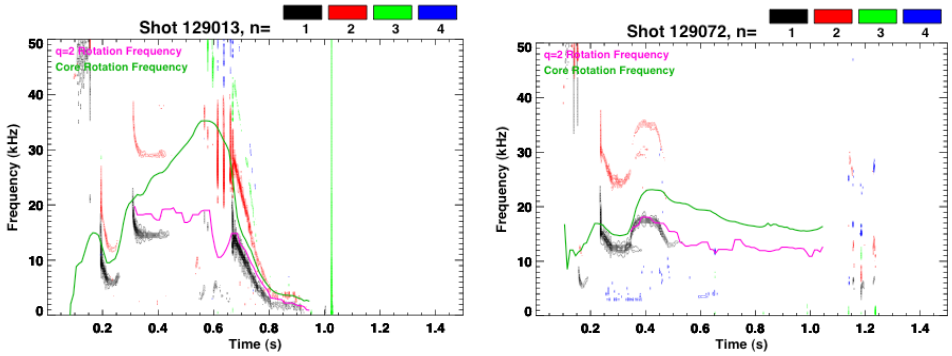

Figure 2.3.4-5: Comparison of low-frequency mode activity in shots without (129013) and with (129072) with lithium evaporation. Also shown are the core (green) and q=2 (magenta) rotation frequencies. The two discharges, designed to determine the effect of lithium evaporation on plasma performance, have all other controlled parameters the same.

The control shot 129013 then develops the large 2/1 mode, the plasma rotation is dramatically reduced, and the shot ultimately disrupts at t=1 sec. after the mode locks. The discharge with DEFC and lithium evaporation shows no sign of the later rotating instability, and ultimately succumbs to a fast-growing external mode, likely a resistive wall mode, at t=1.3 seconds.

The stabilization noted in the above figure was achieved with both lithium evaporation and DEFC; in other more rare cases, one of these two ingredients is sufficient to suppress the mode for the duration of the discharge. A high priority for near-term studies is to understand how the current and rotation profiles with lithium and DEFC change the mode stability, including changes in mode triggering. The studies offer exciting prospects for NTM control, as the liquid lithium divertor and improved dynamic error field correction should allow a significant extension of these high performance discharge regimes.

In the five-year period starting in FY2014, an additional 3 sources will be added to the NSTX NBI system. As discussed in Chapter 6, this upgrade should allow access to fully non-inductive equilibria with $q_{min} > 2$. This scenario would have the effect of eliminating the pernicious m/n = 2/1 and 3/2 resonances from the plasma. The effect of higher order NTMs, such as m/m=3/1 and 5/2, can then be studied. Additionally, the current profile control allowed with the more tangential beams may allow stabilization or mitigation of the NTM through modifications to Δ', in a fashion similar to what was achieved in COMPASS-D [73] with lower-hybrid current drive.

SUMMARY OF RESEARCH PLANS AND TIMELINE

FY2009-11 Complete characterization of NTM onset, including triggering physics and the role of rotation, rotation shear, and small island effects.

FY2009-11 Utilize β_P ramp down experiments to characterize the dependencies of the small island physics on kinetic parameters at low aspect ratio

FY2009-11 Utilize PEST-III for accurate calculations of Δ' in NSTX geometry. Develop solutions to (1) utilizing low-aspect ratio solutions for all terms. Asses merits of low-A for NTM stability

FY2010-12 Implement nonlinear initial value simulations of NTMs with NIMROD and M3D. Compare measured island seeding and evolution to simulations.

FY2012-13 Utilize upgraded NSTX to look for interactions of NTM with fast particles

FY2012-13 Utilize previously developed knowledge base and new tools to develop routine high-β discharges with no deleterious island activity.

2.3.5 Plasma rotation and non-axisymmetric field-induced viscosity

Goal: *Continue to develop quantitative, first-principles physics models of non-axisymmetric field induced plasma viscosity for both resonant and non-resonant fields, and apply results to create new techniques for imparting significant toroidal momentum to the plasma.*

(i) physics and control - results

Plasma rotation can contribute to the stabilization of MHD instabilities by shielding static, three-dimensional error fields and by dissipating free energy available to the instabilities [39, 74]. Sufficient toroidal plasma rotation is required for passive RWM stabilization in NSTX and allows access to the highest β_N operation and the longest pulses in the device. Recent balanced NBI experiments in DIII-D have also shown an increase in energy confinement with increasing plasma rotation [75].

Because of the significant beneficial effects of plasma rotation in tokamaks, it is desirable to maintain plasma rotation in tokamak devices, including ITER, which will have a relatively low source of external momentum input. However, plasma rotation typically slows down in tokamaks during the discharge, likely due to the presence of non-axisymmetric fields from error fields or mode activity. For instance, resonant electromagnetic (EM) torque due to the interaction of device error fields with tearing modes [44, 76] causes the plasma rotation to slow, and magnetic islands to lock, leading to a significant loss in confinement or plasma termination. In addition, non-resonant, non-axisymmetric fields can also lead to substantial rotation damping caused by neoclassical toroidal viscosity (NTV) [77]. This effect was correlated with RWM activity [9,10] and was subsequently verified by quantitative comparison of theory to experiment in NSTX during the past five year period [78].

The plasma rotation profile evolution due to tearing modes is distinct from NTV-induced rotation damping so their lack of influence on rotation drag could be verified. This is illustrated in Figure 2.3.5-1, where the rotation damping observed during application of a non-axisymmetic magnetic field (Figure 2.3.5-1a) is contrasted with rotation damping due to T_{JxB} *on a rotating island* (Figure 2.3.5-1b). The damping due to NTV is relatively rapid, global, and the rotation profile decays in a self-similar fashion. In contrast, the damping due to EM drag is initially localized near the island, and diffusive from this radius, leading to a local flattening of the toroidal plasma rotation frequency, Ω_ϕ, and a distinctive momentum transfer across the rational surface from smaller to larger R as expected by theory [44, 81].

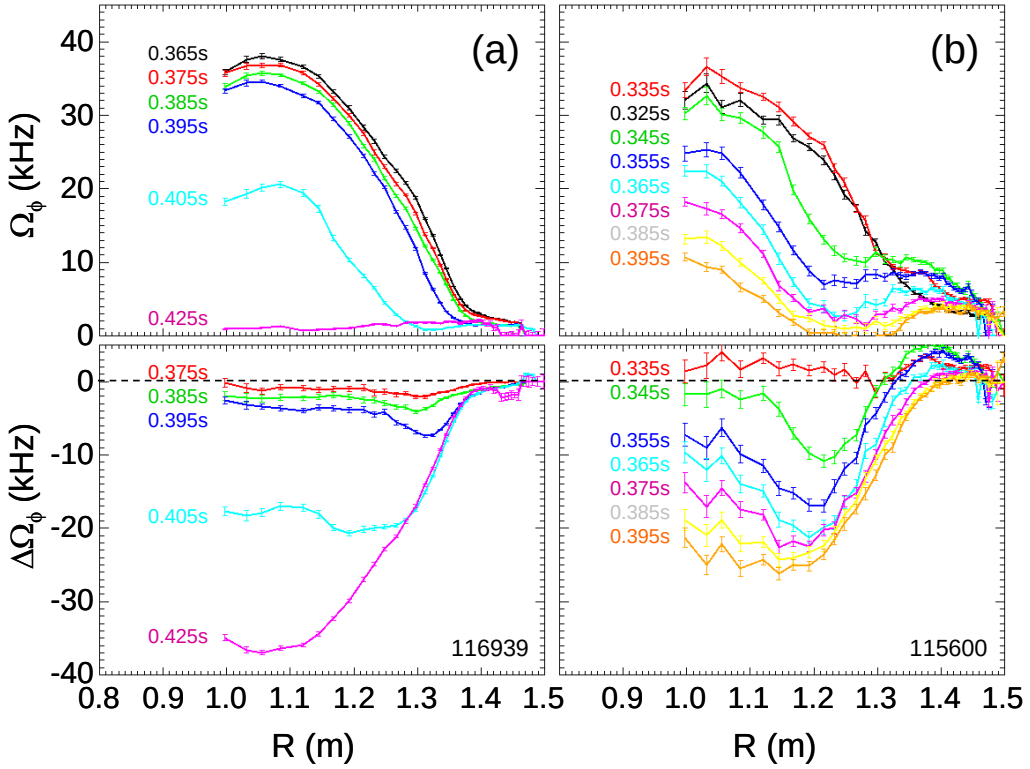

Figure 2.3.5-1 Toroidal plasma rotation profile vs. major radius, and difference between initial profile and subsequent profiles for rotation damping (a) during application of non-axisymmetric field, and (b) during excitation of rotating tearing instability.

Neoclassical toroidal viscosity is caused by the interaction of the plasma with magnetic field components that break the toroidal symmetry of the magnetic confinement field in a tokamak. Using a fluid model, NTV drag can be described as the force on the plasma fluid as it flows through the non-axisymmetric field perturbation. Using a particle model, the drag can be described in a relatively collisional plasma as a toroidal force caused by a radial non-ambipolar flux of particles drifting due to the non-axisymmetric field. In a sufficiently collisionless plasma, the effect is dominated by trapped particle drifts. While the full formulation used for comparison to NSTX experiments can be found in Ref. [78], the dominant flux surface-average force for the present NSTX range of ion collisionality is given by

$$\left\langle \hat{e}_t \bullet \vec{\nabla} \bullet \overleftrightarrow{\Pi} \right\rangle_{(1/\nu)} = B_t R \left\langle \frac{1}{B_t} \right\rangle \left\langle \frac{1}{R^2} \right\rangle \frac{\lambda_{1i} p_i}{\pi^{3/2} \nu_i} (\Omega_\phi - \Omega_{NC}) I_\lambda \qquad (1)$$

where

$$I_\lambda = \frac{\varepsilon^{3/2}}{\sqrt{2}} \left[\int_0^1 d\kappa^2 \left[E(\kappa) - (1-\kappa^2) K(\kappa) \right]^{-1} \sum_n n^2 \left\{ \left[\oint d\theta (\kappa^2 - \sin^2(\theta/2))^{1/2} A_n \right]^2 + \left[\oint d\theta (\kappa^2 - \sin^2(\theta/2))^{1/2} B_n \right]^2 \right\} \right] \qquad (2)$$

$\varepsilon \equiv r/R_0$, and $\lambda_{1i} \equiv 13.708$. The independent integration variable κ is a normalized pitch angle parameter defined in Ref. 79. The functions $K(\kappa)$ and $E(\kappa)$ are the complete elliptic integrals of the first and second kind, respectively, and the Fourier coefficients A_n, B_n for the magnetic field B as defined in Equation (6) of Ref. 78, and Ω_{NC} is the neoclassical toroidal flow velocity [80]. Dedicated NSTX experiments found good quantitative agreement, i.e. ~ O(1), between the measured change in the plasma angular momentum profile during periods of increased non-axisymmetric fields generated by n = 1 and n =3 applied fields, n = 1 RFA, and the n = 1 RWM. As an example, a comparison of the measured dissipation of plasma angular momentum caused by the externally-applied non-axisymmetric fields with the theoretical NTV torque profile is shown in Figure 2.3.5-2 for an n = 3 applied field configuration. The measured value of $d(I\Omega_p)/dt$ includes error bars that take into account the uncertainty in the measured plasma rotation and mass density.

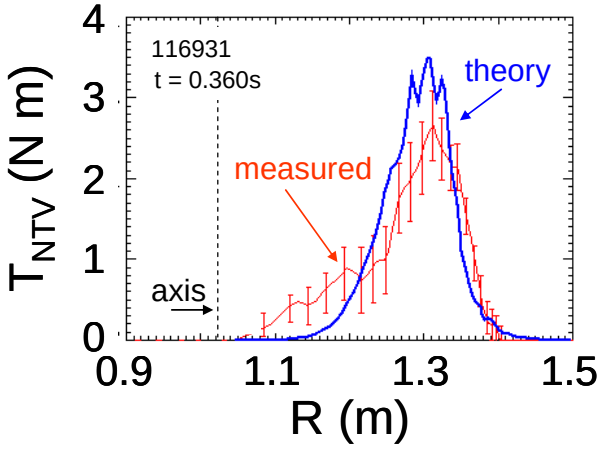

Figure 2.3.5-2 Comparison of measured $d(I\Omega_p)/dt$ profile to theoretical integrated NTV torque for an n = 3 applied field configuration (from Zhu, et al PRL 2006).

The dependence of Equation (1) above on ν_i is expected to saturate as the value becomes much smaller than the trapped ion ExB precession frequency, ω_D. Testing the dependence of NTV torque on ν_i at high beta and low aspect ratio is an important goal to be addressed at the reduced collisionality made possible by the center stack upgrade. This is discussed in the subsection on NTV research plans given below.

Non-resonant $n = 3$ braking has been developed sufficiently to be used as a control tool to reduce toroidal plasma rotation in many NSTX experiments spanning most topical research areas. Although restricted to rotation reduction, this capability has been very useful since co-directed NBI in the device doesn't allow for rotation control with NBI alone. Also, braking with higher-*n* fields is convenient because small changes in applied current can change the plasma rotation by small, predictable amounts, and leads to only a modest reduction to energy confinement, typically less than 10%. Cyclic breaking and spin-up of the plasma rotation has been demonstrated by pulsing the braking field (Figure 2.3.5-3).

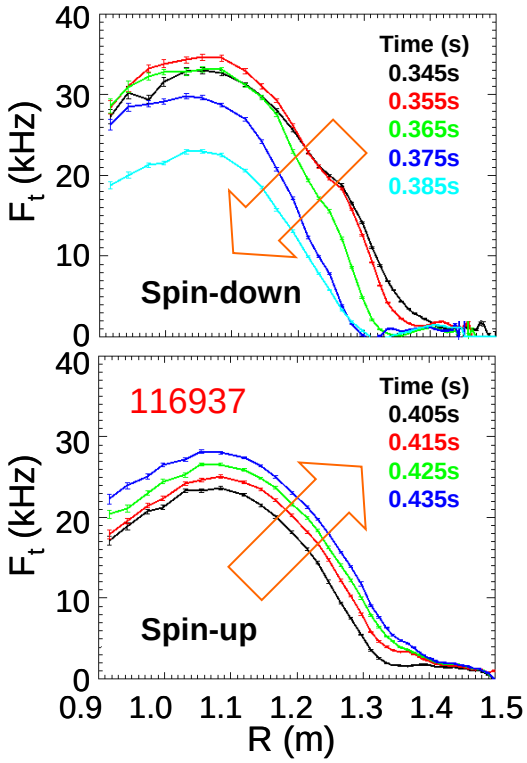

Figure 2.3.5-3 Plasma rotation damping as n = 3 braking is applied, and subsequent plasma spin-up when the braking is released.

To date, the only tool available in NSTX to increase plasma rotation other than the significant toroidal momentum input by neutral beam injection has been dynamic error field correction afforded by the $n = 1$ RWM feedback stabilization system, or open-loop feedback techniques. The observed increases in plasma rotation have been small, but maintenance of plasma rotation can yield significant improvements in plasma pulse length (e.g see Figure 2.3.3-3). However, the success of non-resonant n = 3 braking and its understanding as being generated by NTV opens up the possibility of maintaining or increasing plasma rotation via this physics. This control technique is proposed below for the 2009 – 2013 research period.

(ii) physics and control - plans

First-principles physics understanding of viscosity due to non-axisymmetric fields

It is important to understand the physics of both resonant and non-resonant sources of drag torques to form reliable, first-principle models for future burning plasma and other tokamak experiments. The theory of electromagnetic drag on tearing modes from error fields and NTV drag from non-resonant fields is established, but key questions remain in extrapolation to burning plasma regimes such as in ITER. While the qualitative picture of electromagnetic drag torque fits observations of plasma rotation damping in the presence of tearing modes, there is little first-principle theoretical modeling [81] in toroidal geometry with quantitative comparison to experiment. Therefore, it is unclear whether or not other effects contribute significantly to the torque. For example, the theory of neoclassical toroidal viscosity in the near-field of the island [82] (island NTV, or INTV) might play a significant role in the rotation damping of tearing modes. Since EM, NTV, and INTV drag have different dependencies on plasma parameters (EM scales as $\delta B_{resonant}^2$, NTV scales as $\delta B^2 (p_i/\nu_i)\varepsilon^{1.5}$, and INTV scales as δB (more strongly than NTV) with a more complex dependence on ν_i, understanding each quantitatively is important when scaling to ITER and other future devices. Another important consideration, especially for ITER, is the NTV $1/\nu_i$ scaling. (the so-called "$1/\nu$ regime") as shown in Equation (1), which is appropriate for present NSTX plasmas where the trapped particles are becoming collisionless, $q\omega_E < \nu_i/\varepsilon < \varepsilon^{0.5}\omega_{Ti}$ [80]. Theoretically, NTV is expected to saturate as the ion collisionality drops further, i.e. to significantly below the trapped ion ExB precession frequency. In this regime, which is appropriate for ITER, the $1/\nu_i$ scaling is

theoretically expected to become $\nu_i/(\nu_i^2 + \omega_E^2)$, but this has not been experimentally demonstrated. Experiments conducted in the 2009 – 2013 period will investigate the key scalings of the important physical mechanisms described above that lead to plasma rotation damping, with particular emphasis on the dependence of NTV torques on ion collisionality once the center stack upgrade is made. The IPEC code will be an important tool for this study, determining the impact of non-axisymmetric field amplification or shielding on the perturbed field used in the NTV torque calculations.

Toroidal momentum input from propagating, non-resonant fields

The present physics understanding of NTV may allow a new practical tool for maintaining or increasing plasma rotation by means other than neutral beam momentum input, without exciting strong tearing modes and/or leading to a reduction in energy confinement. The application is of critical importance to future devices with low toroidal momentum input (e.g. burning plasma devices such as ITER) that could benefit from increased rotational stabilization of MHD modes and may synergistically aid ELM mitigation. Quantitative agreement between NTV theory and experiment on NSTX to date supports the idea of controlling the plasma toroidal rotation by applying toroidally phased fields with $n > 1$ and relying on the NTV from the propagating, non-resonant field components to apply positive momentum to the plasma, enabling the plasma to be spun-up as well as spun down.

The technique of using propagating field-driven NTV for robust maintenance of plasma rotation via non-resonant rotating fields has many advantages. The technique can be applied in principle to any toroidal device in which NTV is significant (relatively low collisionality plasmas), including future burning plasma experiments such as ITER. The technique is relatively simple – a toroidally propagating, non-resonant field is applied to the plasma, and NTV drags the plasma in which the field penetrates up to the rotation speed of the applied field. The most basic implementation does not require feedback or a sophisticated control system.

In NSTX, the newly proposed NCC can do triple-duty by supplying the propagating non-resonant field for this research. With 12 internal toroidal coils, $n = 2$ or $n = 3$ fields can be made to propagate. With $n > 1$, the most deleterious $n = 1$ resonant modes, both tearing modes and RWMs, will not be excited. This has been demonstrated in NSTX already in that $n = 3$ fields used for slowing the plasma do not directly excite these modes. If magnetic islands form in the region of the applied field, the NTV torque will supplement the NBI torque in counteracting the tendency of the mode to lock. Also, the radial footprint of the NTV torque is radially wider than electromagnetic torques caused by propagating resonant fields. Although the technique is not specific to NSTX, the device is an excellent facility to run the research since the applied torque scales as $(1/A)^{1.5}$ (see Equation (1)). Low-cost audio amplifiers may be sufficient to generate the field amplitude and propagation frequencies needed. Having the ability of at least maintaining 5 kHz rotation speeds near the q = 2 surface should yield a sufficient proof-of-principle and give reasonable flexibility to conduct physics research (of course, a higher frequency ~ 10 kHz would be even better). A full design study is required, but this should be possible with $n = 2$ fields, and the desired $n = 3$ may also be possible. The system would also allow research using the resonant $n = 1$ field, so that the effects of resonant fields could be evaluated, and also to make important comparisons with the existing tokamak research in this area. For instance, TEXTOR has demonstrated spin up of $n = 1$ tearing modes using $n = 1$ fields up to 3.75 kHz [83,84] and JFT-2M has demonstrated a local increase in plasma rotation due to the EM transfer of momentum from the $n = 1$ field to an $m = 2$, $n = 1$ magnetic island [85].

Application of NTV momentum input to the plasma, while relatively simple in principle, requires that a practical system be designed, constructed and demonstrated to determine if certain potential issues can be addressed. Propagating $n > 1$ fields requires higher frequency, f, to generate the same phase velocity, since toroidal phase velocity ~ f / n. The need to use higher frequencies presents issues with field penetration. Also, the higher n sideband fields won't propagate unidirectionally, therefore higher order n sidebands should be kept small. For the present RWM coil on NSTX, the NTV due to $n \neq 3$ is relatively small, with the $n = 9$ being the largest sideband. An NCC design with 12 coils should place the majority of the NTV torque into the $n = 2$ and $n = 3$ component. This will be evaluated during the physics design of the system.

Real-time control of plasma rotation

Real-time control of plasma rotation will be useful in NSTX, as well as in other future devices envisioning solely high plasma rotation due to co-directed NBI (KSTAR, CTF). With the new NCC, the following directly controlled sources and sinks of plasma toroidal momentum on NSTX will be:

Sources:
1) Neutral beam injection
2) Resonant field propagation momentum (NCC)
3) Non-resonant field propagation (NCC)

Sinks:
1) Static resonant field (NCC, external RWM coils)
2) Static non-resonant field (NCC, external RWM coils)

In the nearer term, the plan calls for a 2nd SPA in FY11. This will allow n=1 DEFC/RWM feedback at the same time as n=2 & 3 fields are utilized for rotation control. Given that the n=2 and 3 fields from the RWM coils yield different radial profiles of damping (due to the different radial variations of the fields), this should allow some localization of the damping, and hence basic rotation control. This feature, i.e. simultaneous and independent n=1,2,&3 fields, is thus useful for both RMP (chapter 5) and rotation control.

The design of the NCC will then aim at producing a field spectrum that yields a different radial footprint of non-resonant NTV than that produced by the existing external RWM coils. Therefore, rotation profile control will be possible by using both sets of coils.

These sources and sinks can be used in a feedback loop to control the plasma rotation magnitude and profile. Such control can be used to examine a greater range of rotation profiles for future MHD stability studies.

Real-time charge exchange recombination spectroscopy (CHERS) will be implemented as the primary sensor for such a system at two or three radial positions in the 2009 – 2013 time frame. After successful interface of these measurements with the PCS, control system software will be developed that will allow control of the sources and sinks of toroidal plasma momentum. Basic capability of this system is envisioned in the next five years, which is planned to include NBI for source control, and the external RWM coil for sink control. The sources and sinks due to the NCC will be implemented as they are tested, but are not envisioned to be implemented in the feedback loop in the 2009 – 2013 period.

SUMMARY OF RESEARCH PLANS AND TIMELINE

FY2009-11 Expand physics understanding of plasma viscosity induced by resonant and non-resonant field sources (applied fields and MHD modes), determining the plasma response with experimental data and IPEC. Focus on examining key parameters for future tokamak devices such as ion collisionality, q, and β_N. Test NTV theory quantitatively using $n = 2$ applied field. Perform design study of NCC for use as source and sink of toroidal momentum.

FY2010-12 Utilize reduced collisionality plasmas using new center stack to controllably access $1/\nu$ and lower collisionality regimes of NTV theory. Compare to NTV theory including more consistent collisionality connection formulae and kinetic simulations of NTV flow-damping.

FY2011-12 Demonstrate n=2 & 3 NTV for rotation magnitude and profile

FY2011-12 Demonstrate the use of the NCC (incremental) as a momentum sink using both resonant and non-resonant static field and quantitatively compare to NTV theory for verification. Subsequently, attempt use of the NCC as a momentum source using both resonant and non-resonant fields as suitable power supplies become available.

FY2011-12 Demonstrate real-time plasma rotation control using rtCHERS sensors and basic sources and sinks of plasma toroidal momentum input (NBI, $n = 3$ non-resonant NTV drag using external RWM coil).

FY2013 Demonstrate real-time plasma rotation control using full complement of toroidal momentum sources and sinks, including the NCC.

2.3.6 Disruption physics, consequences, avoidance, and prediction.

Goal: *Characterize the effects of disruptions at low aspect ratio and high beta by measuring halo currents and thermal and current quench characteristics. Develop methods to predict disruptions and mitigate their impact.*

(i) Understanding the consequences of disruptions in an ST plasma

Disruptions can quickly eliminate the entire thermal energy and quench the total plasma current in a tokamak/ST facility like NSTX, resulting in impulsive heat loads to plasma facing components and large forces on in-vessel structures. While disruptions do not generally have operational consequences in NSTX for the present parameters, the device represents a unique environment for the study of disruption physics. These studies began in earnest in the 2007, with the initiation of a detailed examination of existing NSTX data for disruption characteristics, particularly the dynamics of the plasma current quench [86], and continued into 2008 with the installation of a devoted halo current detection system. Studies in the coming research period will continue this effort, with a particular focus on the dynamics of the thermal quench and halo currents. This data will provide valuable contributions to the updated ITPA disruption database [87], and provided critical design data for future low aspect ratio devices such as NHTX or a CTF. Disruption control will be addressed through the implementation of disruption prediction algorithms, and techniques to mitigate the effects of disruptions will be addressed.

The process leading up a disruption typically begins with some MHD mode or control failure [88]. This event typically leads to a degradation of confinement, often including loss of H-mode, for a period of time before the actual disruption. The energy loss during this precursor phase is of great importance, as energy lost slowly during this period will not be present to contribute to loading during the thermal quench [89]. Results from NSTX have demonstrated substantial energy loss in this pre-disruptions phase, as indicated by the histograms in Fig 2.3.6-1. This data was taken from a database of ~800 disruptions spanning the operational lifetime of the device, selected for having large quench rates, large values of stored energy before the disruption, or large halo currents. The blue curve shows a histogram for the maximum stored energy during the discharge; there are values at low stored energy, corresponding to disruptions during the current ramp or shots with low heating power, and at high stored energy, for instance in high-β experiments. The distribution of pre-disruption energies is, however, weighted strongly to low energy, and there are no cases found with stored energy >250kJ immediately before the disruption. This result bodes well for future large ST devices, as it implies that the full flat-top stored energy will usually not be present for the thermal quench. The extension of the NSTX operating regime to higher fields, currents, and stored energy will be critical in establishing whether the trend will hold for larger devices.

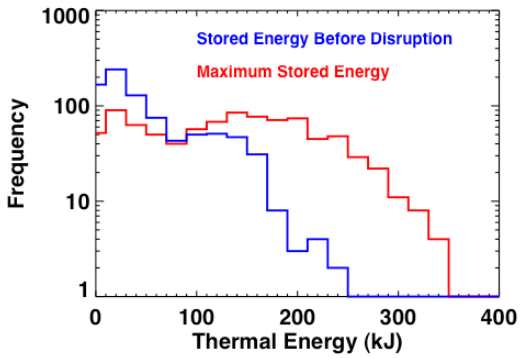

Figure 2.3.6-1 ***The area-normalized current quench time for discharges in the NSTX disruption database, as well as the suggested limit for ITER.***

Whatever thermal energy remains after this precursor phase is very rapidly lost to the wall during the thermal quench phase, either through radiation or conduction. This is of great concern in a burning plasma, where a significant fraction of the first wall material can be melted/ablated in each event [90]. There is not, however, general agreement regarding the broadening of the power deposition profile during

this phase: the ITER physics basis assumes a broadening of 1-10 times the equilibrium SOL heat deposition width, though results from, for instance, ASDEX upgrade [91] or JET [92] show substantially greater broadening of the SOL during a disruption. This creates significant uncertainty in extrapolation to divertor heat loading in larger devices. Indeed, the load in the divertor may be less than feared, but the loading of the first wall may be unacceptably large [92]. NSTX has not in the past had the diagnostics to address this issue. However, a fast IR camera was recently purchased for the study of transient power loading events, allowing this to be an important area of focus for future research. This camera, coupled to soft X-ray measurements, should allow an accurate assessment of the time-scale of the thermal quench and it's associated heat pulse, as well as the spatial distribution of the lost energy. An important focus of these studies will be to understand which, if any, plasma configurations lead to disruptions with the largest heat loading.

The thermal quench is followed immediately by the current quench, often resulting in large eddy current induced forces and torques on nearby conducting structures [93]; this subject has been the focus of a recent study in NSTX [86]. A key finding of these studies, first identified in the context of ITPA Disruption Database Activities [ii], is that the maximum current quench rates in NSTX are, on an area normalized basis, up to four times faster than in conventional aspect ratio tokamaks. This is clearly demonstrated in Fig 2.3.6-2, where the NSTX disruption data implies a minimum quench time of 0.4 msec/m^2, compared to the a suggested ITER limit of 1.7msec/m^2 [iii]. The faster quenches in NSTX, and STs in general, can likely by understood as an L/R decay effect, where L is the effective inductance of the plasma torus and R is the resistance of the cold plasma. Using an inductance $L_P^{eff} = \mu_0 R_0 \left[\ln\left(8/\sqrt{\kappa\varepsilon} \right) - 7/4 \right]$ yields an area normalized decay time of

$$\frac{\tau_{L/R}}{S} = \frac{\mu_0}{2\pi\eta}\left[\ln\left(8/\sqrt{\kappa\varepsilon} \right) - 7/4 \right].$$

The term in brackets is 4-5 times smaller for a highly elongated ST than a conventional aspect ratio tokamak at moderate elongation, potentially explaining the difference in quench rates.

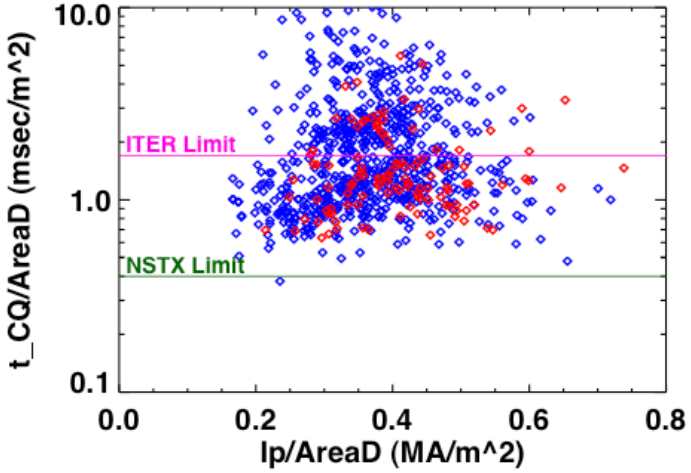

Figure 2.3.6-2 ***The area-normalized current quench time for discharges in the NSTX disruption database, as well as the suggested limit for ITER. Blue points correspond to discharges that disrupt during the I_P flat top or rampdown, and red points to those that disrupt during the current ramp.***

The process of disruption is often coupled to loss of vertical position control; this can happen in the period between the MHD precursor and the thermal quench, after the thermal quench itself, or when the loss of vertical control and subsequent plasma-vessel contact initiates the disruption. When contact is made between the plasma and plasma facing components, currents can flow that link both the plasma edge (the halo) and nearby PFCs. These "halo currents" can result in large forces on the in-vessel components [94]; they are, for instance, anticipated to be the dominant source of electromagnetic loading during slow current quenches in ITER [90]. In response to ITPA requests, and the anticipated design needs for future ST facilities, NSTX has begun a program to measure and understand halo currents.

This effort began with the implementation of a set of halo current detectors in the lower divertor for the FY08 research campaign. These are composed of two toroidal arrays of individual B_T, six sensors per array, functioning as sections of a partial Rogowski coil. They can measure both the magnitude and toroidal peaking of currents flowing in the lower vessel, and can be used to assess the net current flowing into the outboard divertor. These are complemented by previously installed lower center-column halo current measurements via Rogowski coils and measurements of the currents flowing from the inner to outer vessels through the torus grounding system.

These efforts during the FY08 physics campaign have proved highly successful, measuring halo currents that had previously gone unnoticed and revising upward estimates for halo current fractions in NSTX. A sample of this data is shown in Fig 2.3.6-3, which shows maximum halo currents, as a function of I_P^2/B_T, for four different current paths. The blue and red points, corresponding to the currents in the lower center-stack and busswork linking the inner and outer vessel respectively, show maximum halo currents of 40-50 kA. Similar data has existed for a few years and implied halo current fractions of ~5%, with little dependence on I_P or B_T. The newly available dark green and turquoise points, corresponding to the current flowing in the lower vessel near the CHI gap and the net current into the lower outboard divertor, show substantially larger halo currents, with a clear I_P^2/B_T scaling as noted on Alcator C-MOD [95]. The points nearest the bounding lines are for deliberate VDEs with I_P^2/B_T <1.2 MA^2/T, and represent a factor of ~5 increase in the measured halo current with the new instrumentation. Note that for the upgraded NSTX (I_P=2MA, B_T=1T), this scaling implies ~380kA of halo current flowing in the lower vessel and a factor of four increase in the expected halo current JxB loading of in-vessel components.

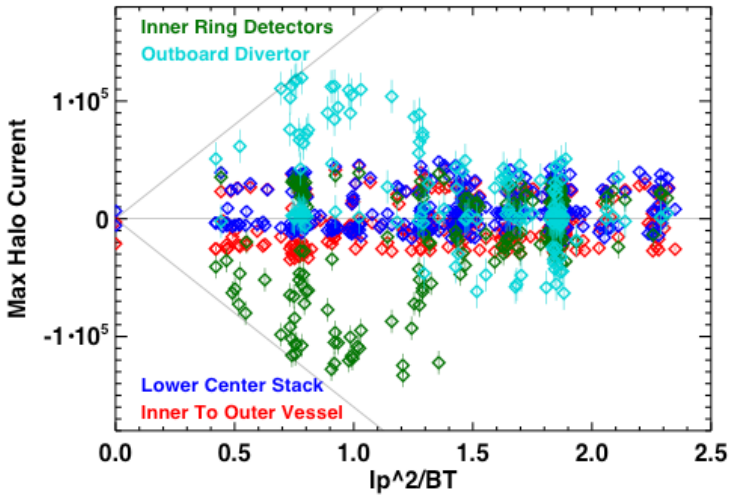

Figure 2.3.6-3: The maximum halo current, as a function of I_P^2/B_T, for different paths in the device.

One assumption in the ITER design is that the maximum halo current and eddy current load will not occur simultaneously; this is based on, for instance, JET results demonstrating the larger halo currents for discharges with slower quench rates [96]. The trend observed in NSTX is exactly the opposite: as shown in Fig. 2.3.6-4, the envelope of halo currents, in this case detected flowing in the vessel bottom near the

CHI gap, scales linearly with the I_P quench rate, in agreement with the notion that the voltage due to the toroidal and poloidal flux decay drives the halo current. This and similar information is critical in performing design tasks for next-step ST experiments.

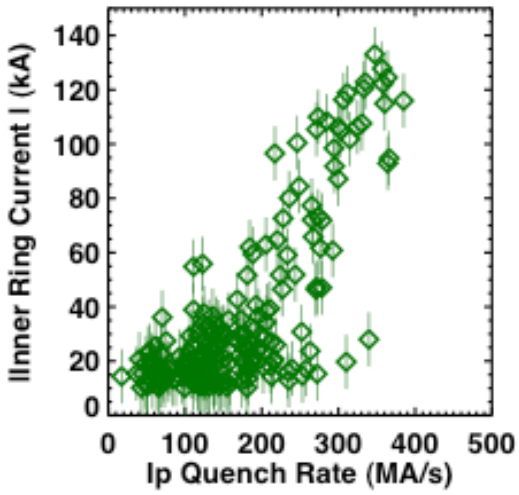

Figure 2.3.6-4: Halo current magnitude in the vessel near the CHI gap vs. the plasma quench rate. The largest halo currents often occur for the fastest quenches.

While the present halo current detection upgrades have proven successful, they leave many questions open. In particular, this system measures only the net current flowing into the lower divertor; currents that flow into and then out of the lower divertor are not detected. In this sense, the measurements presented above are *lower bounds* on the halo current magnitude. In order to resolve the local currents in the divertor more clearly, the magnetic diagnostics for halo currents will be augmented by instrumented tiles during this research period [97]. The first set of these instrumented tiles will be installed on the outboard divertor during the fy09-fy11 period, as part of the upgrade for the liquid lithium divertor (LLD). These will likely include both toroidal and radial arrays of tiles. These will be supplemented with measurements of the currents flowing into the LLD segments. The machine modifications associated with the center-stack upgrade will then be utilized to install instrumented tiles on the inner divertor. These tiles arrays will allow the local halo current sources and sinks in the divertor to be accurately measured and provide greater spatial resolution for measurements of local peaking factors. More speculatively, the sensitive measurements allowed by the instrumented tiles may allow a connection to be drawn between SOLC

currents during pre-disruption mode growth and halo currents during disruption, potentially allowing more detailed understanding of the mode physics leading to halo current peaking [98]. Note that during the equilibrium phase of the discharge, these instrumented tiles will be utilized to measure equilibrium SOL currents, as described in section 2.3.2.

(ii) Disruption prediction, avoidance, and mitigation

Disruption control has typically been addressed through three steps: i) avoiding the discharge configurations and underlying instabilities that lead to disruptions, ii) detecting the approach to a disruption, and iii) implementing a either soft-stop or fast shutdown procedure to mitigate the damaging effects. Substantial progress has been made in the last area via Massive Gas Injection (MGI) [99] in DIII-D and C-MOD, with results that should be broadly applicable to the ST as well.

The research presented in the other sections of this MHD chapter, and to a lesser extent in the control chapter, is largely devoted to understanding and controlling the MHD instabilities that lead to disruptions. By developing discharge designs and control techniques that avoid or mitigate instabilities like low-density locked modes, RWMs and NTMs, it should be possible to reduce disruptivity at high β_N. The implementation of NBI control for β_N feedback in FY09 should allow comfortable operation closer to limits, i.e. compensate for transients in confinement that otherwise would result in too-high values of beta. Continued improvements in DEFC and RWM feedback will allow better maintenance of stabilizing rotation in high-β plasmas. Furthermore, the potential exists to use the RWM coils to generate traveling waves and the in-vessel sensors to detect the RFA plasma response in real time; this active MHD spectroscopy scheme would allow NBI control based on proximity to the no-wall β limit.

However, even with these planned improvements, disruptions will occur when expanding operation boundaries, as well as due to machine infrastructure malfunctions; this provides an opportunity to test methods that predict the onset of disruptions in an ST. NSTX has an ever-expanding set of real-time measurements that can be used to monitor and predict disruptive behavior. Present capabilities include real-time equilibrium reconstructions with rtEFIT, yielding quantities like β_N, q_{95}, l_i and accurate reconstructions of the plasma position, and real-time detection of resistive wall modes and locked modes.

These will be expanded during this research period to include real-time measurements of plasma rotation from CHERS and non-axisymmetric mode growth from dedicated USXR arrays. Specific additional real-time measurements, such as radiated power and detection of large rotating modes, can be easily added as the need arises.

These diagnostics and capabilities will be used in order to develop disruption prediction methods. Neural-net algorithms have proven successful in predicting impending disruptions in conventional aspect-ratio tokamaks [100], and are a likely method for disruption prediction in ITER [88]; these methods have never been implemented at low-A. However, other unique precursors can be studied in NSTX, including RFA growth from active MHD spectroscopy and non-magnetic detection of locked modes and RWMs. The relative merits of single-signal vs. neural net detection will be examined, and efforts will be made to determine the minimal set of precursor signals for reliable disruption prediction in a high-β ST.

With the more aggressive parameter regime for the upgraded NSTX, it will likely be advantageous to attempt some mitigation techniques in order to reduce thermal and mechanical stresses on components. The previously mentioned disruption prediction research will then naturally lead to disruptions mitigation research. These will likely include simple techniques like deshaping of the plasma, reducing the heating power, and preemptively ramping down the plasma current, all of which can be relatively easily implemented with the flexible NSTX control system. More aggressive mitigation strategies, including noble gas injection, will be implemented if the physics program and engineering constraints mandate them.

SUMMARY OF RESEARCH PLANS AND TIMELINE

FY2009-11 Design and test prototype instrumented tiles in the outboard divertor, for SOL and halo current measurements. Install array on outboard divertors to enable complete assessment of halo current there

FY2009-10 Implement fast IR camera for studies of PFC loading during the disruption thermal quench. Quantify the time-scale and heat distribution against relative plasma parameters and disruptions type, if possible.

FY2010-11 Study techniques for the detection of impending disruptions, utilizing techniques such as neural nets, based on quantities measured in real-time on NSTX. Develop strategies to mitigate these disruptions.

FY2011-12 Implement instrumented tiles on the inboard divertor as part of the center-stack upgrade. This should allow near complete measurements of halo currents in NSTX.

FY2012-13 Test mitigation strategies in upgraded NSTX plasmas. Determine how previously measured disruption characteristics extrapolate to I_P=2MA, B_T=2T configurations.

2.4 Timeline for Research Goals FY2009-2013

The proposed research program time line for macroscopic stability for 2009-2013 is shown below.

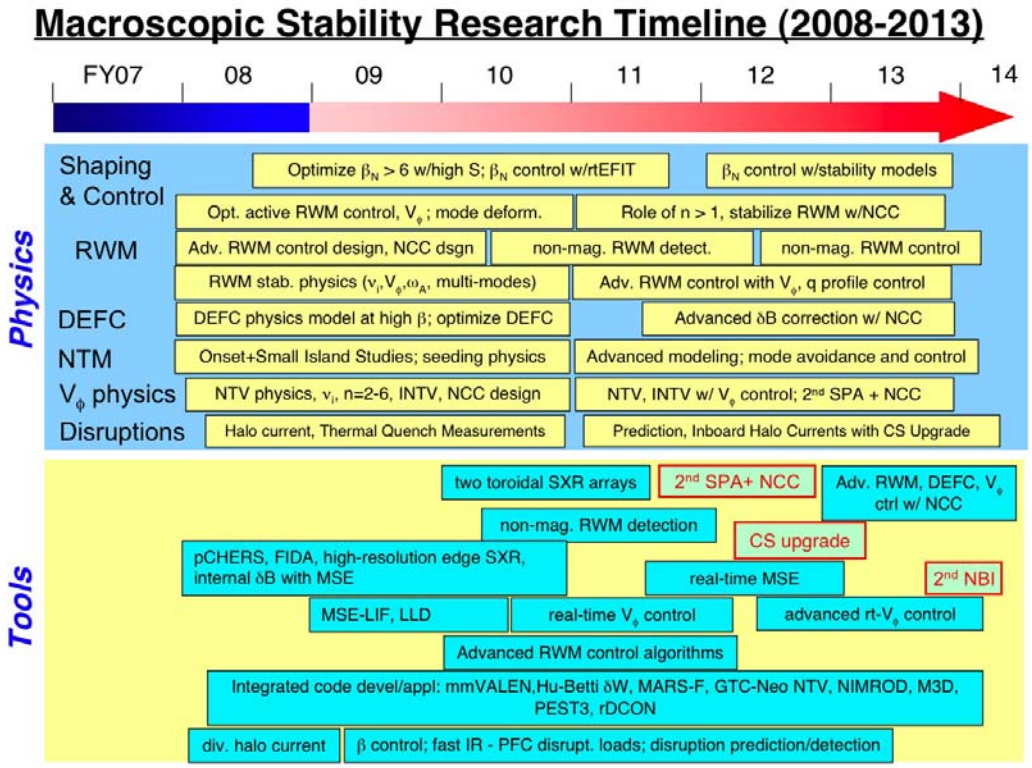

2.5 References

[1] E. Strait, Phys. Plasmas **1**, 1415 (1994).

[2] S.A. Sabbagh, *et al.*, Phys. Fluids B **3**, 2277 (1991).

[3] Howl, W. *et al.*, Phys. Fluids B **4**, (1992) 1724.

[4] Strait, E.J. et al., Phys. Rev. Lett. 74, (1995) 2483.

[5] Turnbull, A.D. *et al.*, Phys. Rev. Lett. **74** (1995) 718.

[6] Menard, J.E. *et al.*, Nucl. Fusion **37** (1997) 595.

[7] Peng, Y.-K.M. and Strickler, D.J., Nucl. Fusion **26** (1986) 769.

[8] Stambaugh, R.D. *et al.*, Fusion Technology **33** (1998) 1.

[9] S.A. Sabbagh, et al., Phys. Plasmas **9**, (2002) 2085.

[10] S.A. Sabbagh, J.M. Bialek, R.E., Bell, et al., Nucl. Fusion **44**, 560 (2004).

[11] J.E. Menard, R.E. Bell, E.D. Fredrickson, et al., Nucl. Fusion **45**, 539 (2005).

[12] J.E. Menard, R.E. Bell, D.A. Gates, et al., Phys. Rev. Lett. **97**, 095002 (2006).

[13] H. Reimerdes, T.C. Hender, S.A. Sabbagh, et al., Phy. Plasmas **13**, 056107 (2006).

[14] F. Najmabadi and the ARIES Team, Fus. Eng. Design **65**, 143 (2003).

[15] Y.-K. M. Peng, P.J. Fogarty, T.W. Burgess, et al., Plasma Phys. Controll. Fusion **47**, B263 (2005).

[16] T.K. Mau, S.C. Jardin, C.E. Kessel, et al. Proc. 18th IEEE/NPSS Symp. on Fus. Eng. (Albuquerque, NM) 1999 pp 45-48.

[17] S.A. Sabbagh, et al., Nucl. Fusion **41**, 1601 (2001).

[18] D.A. Gates, J.E. Menard, R. Maingi, et al., *Nucl. Fusion **47**, 1376 (2007)*

[19] D.A. Gates, and the NSTX National Research Team, Phys. Plasmas **10**, 1659 (2003).

[20] A. Bondeson and D.J. Ward, Phys. Rev. Lett. **72**, 2709 (1994).

[21] H. Reimerdes, et al., Phys. Rev. Lett. **93**, 135002 (2004).

[22] Sabbagh, S.A., Sontag, A.C., Bialek, J.M., et al., Nucl. Fusion **46**, 635 (2006).

[23] Glasser, A.H. and Chance, M.C., Bull. Am. Phys. Soc. **42**, 1848 (1997).

[24] Sontag, A.C., Sabbagh, S.A., Zhu, W., et al., Phys. Plasmas **12,** 056112 (2005).

[25] Boozer, A.H., Phys. Rev. Lett. **86**, 5059 (2001).

[26] Garofalo, A.M., Jensen, T.H., and Strait, E.J., Phys. Plasmas **10**, 4776 (2003).

[27] Reimerdes, H., Chu, M.S., Garofalo, A.M., et al., Phys. Rev. Lett. **93**, 135002 (2004).

[28] J.M. Bialek , et al., Phys. Plasmas **8**, 2170 (2001).

[29] A.H. Glasser and M.C. Chance, Bull. Am. Phys. Soc. **42**, 1848 (1997); W. Newcomb, Ann. Phys. **10**, 232 (1960).

[30] D. Stutman, et al., Rev. Sci. Instrum. **74**, 1982 (2003).

[31] M. Okabayashi, et al., Phys. Plasmas **8**, 2071 (2001).

[32] M. Chu, et. al., Nucl. Fusion, **43**, (2003) 441.

[33] E.J. Strait, et al, Phys. Plasmas **11**, 2505 (2004).

[34] S.A. Sabbagh, R.E. Bell, J.E. Menard, et al., *Phys. Rev. Lett.* **97**, 045004 (2006).

[35] P.R. Brunsell, et al., Plasma Phys. Control. Fusion **47**, B25 (2005).

[36] Y. In, J.S. Kim, D.H. Edgell, et al., Phys. Plasmas **13**, 062512 (2006).

[37] H. Takahashi, E.D. Fredrickson, M.J. Schaffer, Phys. Rev. Lett. **100**, 205001 (2008).

[38] O.N. Katsuro-Hopkins, J.M. Bialek, D.A. Maurer, et al., Nucl. Fusion **47**, 1157 (2007).

[39] Fitzpatrick, R., Phys. Plasmas **9**, 3459 (2002).

[40] H. Reimerdes, A.M. Garofalo, G.L. Jackson, et al., Phys. Rev. Lett. **98**, 055001 (2007).

[41] A. Bondeson and M.S. Chu, Phys. Plasmas **3**, 3013 (1996).

[42] A.M. Garofalo, G.L Jackson, R.J. LaHaye, et al., Nucl. Fusion **47**, 1121 (2007).

[43] R. Fitzpatrick, Nucl. Fusion 2007.

[44] R. Fitzpatrick, Nucl. Fusion **33**, 1049 (1993).

[45] K.C. Shaing, Phys. Plasmas **11**, 5525 (2004).

[46] B. Hu and R. Betti, Phys. Rev. Lett. **93**, 105002 (2004).

[47] B. Hu, R. Betti, and J. Manickam, Phys. Plasmas **12**, 057301 (2005).

[48] J.-K. Park, A. H. Boozer, and A. H. Glasser, Phys. Plasmas 14, 052110 (2007).

[49] J.-K. Park, M. J. Schaffer, J. E. Menard, and A. H. Boozer, Phys. Rev. Lett. 99, 195003 (2007).

[50] T.C. Hender et al., Progress on the ITER Physics Basis (Chapter 3), Nucl. Fusion **47**, S128 (2007).

[51] D.A. Gates, et al., APS 2000 – NTM observation in NSTX reference.

[52] R. Buttery, et al., Phys. Rev. Lett **88**, 125005 (2002).

[53] Z. Chang and J.D. Callen, Nuclear Fusion **30**, 219 (1990).

[54] R. Fitzpatrick, Phys. Plasmas **2**, 825 (1995).

[55] F. L. Waelbroeck, J.W. Conner, and J.R. Wilson, Phys. Rev. Lett. **87**, 215003 (2001).

[56] S. Kruger, C.C. Hegna, and J.D. Callen, Phys. Plasmas **5**, 455 (1998).

[57] R.J. La Haye, et al, Nuclear Fusion **46**, 451 (2006).

[58] H. Reimerdes, Phys. Rev. Lett **88**, 105005 (2002).

[59] D. Brennan, et al, Phys. Plasmas **10**, 1643 (2003).

[60] R.J. La Haye, Phys. Plasmas **13**, 055501 (2006).

[61] R.J. Buttery et al., *20th IAEA Fusion Energy Conference*, (Vilamoura, Portugal 2004), paper IAEA-CN-116/EX/7-1, Conference & Symposium Papers CD ROM, IAEA-CSP-25/CD, ISBN 92-0-100405-2, ISSN 1562-4153, IAEA Vienna (2005).

[62] M. Maraschek, et al, Plasma Phys. Control Fusion **45**, 1369 (2003).

[63] R. J. Buttery, et al, *Rotation and Shape dependence of Neoclassical Tearing Mode thresholds on JET*, 28th EPS Conference on Contr. Fusion and Plasma Phys. 2001.

[64] R. Buttery, et al, Phys. Plasmas **15**, 056115 (2008).

[65] E. Fredrickson, Phys. Plasmas **9**, 548 (2002).

[66] A. Gude, S. Gunter, S. Sesnic, and the ASDEX upgrade Team, Nuclear Fusion **39**, 127 (1999).

[67] S. Sesnic, et al, Phys. Plasmas **7**, 935 (2000).

[68] S.E. Kruger, PhD Thesis, The University of Wisconsin - Madison (1999).

[69] Chandra, Nucl. Fusion **45**, 524 (2005).

[70] X.L. Chen and P.J. Morrison, Phys. Fluids B **4**, 845 (1992).

[71] D.P. Brennan, A.D. Turnbull, M.S.Chu, R.J. La Haye, L.L. Lao, T.H. Osborne and S.A. Galkin, General Atomics Report A25648, Phys. Plasmas **14**, 056108 (2007).

[72] A.L. Rosenberg, et al, Phys. Plasmas **9**, 4567 (2002).

[73] C.D. Warrick, et al, Phys. Rev. Lett **85**, 574 (2000).

[74] R. Betti and J.P. Friedberg, Phys. Rev. Lett. **74**, 2949 (1995).

[75] W. Solomon, et al., Plasma Phys. Controll. Fusion **49** No 12B, B314 (2007).

[76] E. Lazzaro, et al., Phys. Plasmas **9**, 3906 (2002).

[77] K.C. Shaing, S.P. Hirschman, and J.D. Callen, Phys. Fluids **29**, 521 (1986).

[78] W. Zhu, S.A. Sabbagh, R.E. Bell, et al., Phys. Rev. Lett. **96**, 225002 (2006).

[79] K.C. Shaing, Phys. Plasmas **10**, 1443 (2003).

[80] A.J. Cole, C.C. Hegna, J.D. Callen, Phys. Plasmas **15**, 056102 (2008).

[81] M. Yokoyama, et al., Nucl. Fusion **36**, 1307 (1996).

[82] K.C. Shaing, PRL **87**, 245003 (2001).

[83] R.C. Wolf, W. Biel, M.F.M. deBock, et al., *20th IAEA Fusion Energy Conference*, (Vilamoura, Portugal 2004), paper IAEA-CN-116/EX/6-5 Conference & Symposium Papers CD ROM, IAEA-CSP-25/CD, ISBN 92-0-100405-2, ISSN 1562-4153, IAEA Vienna (2005).
[84] H.R. Koslowski, Y. Liang, A. Krämer-Flecken, et al., Nucl. Fusion **46**, L1 (2006).
[85] K. Oasa, H. Aikawa, Y. Asahi, et al., Proc. 15th Int. Conf. On Plasma Phys. and Controll. Nucl. Fusion Research (Seville, Spain 1994) (IAEA) vol. 2 p. 279.
[86] S. P. Gerhardt et al, "Characterizations of the plasma current quench during disruption in the National Spherical Torus Experiment", submitted to Nuclear Fusion.
[87] J.C. Wesley et al. , *21st IAEA Fusion Energy Conference* (Chengdu, China 2006), paper IT/PI-21.
[88] T.C. Hender, et al., Nuclear Fusion **47**, S128 (2007).
[89] V. Ricardo, A. Loarte, and the JET EFDA Collaborators, Nuclear Fusion **45**, 1427 (2005).
[90] M. Sugihara et al., Nucl. Fusion **47**, 337 (2007).
[91] G. Pautasso, et al., 31st European Physical Society Conference on Plasma Physics, London, 2004, Paper P-4.132.
[92] G.F Mathews, et al, Nuclear Fusion **43**, 999 (2003).
[93] M. Sugihara, V. Lukash, Y Kawano, R. Yoshino, Y. Gribov, R. Khayrutdinov, N. Miki, J. Ohmori, and M. Shimada, J. Plasma Fusion Res. **79**, 706 (2003).
[94] V. Ricardo, S. Walker, and P. Noll, Nucl. Fusion **42**, 29 (2000).
[95] R. S. Granetz, et. al., Nuclear Fusion **36**, 545 (1995).
[96] V. Riccardo, et al, Nuclear Fusion **46**, 925 (2004).
[97] M.J. Schaffer & B.J. Leikind, Nuclear Fusion **31**, 1750 (1991).
[98] N. Pomphrey, et al., Nucl. Fusion **38**, 449 (1998).
[99] R.S. Granetz et al., Nucl. Fusion **47**, 1086 (2007).
[100] C.G. Windsor, et al., Nucl. Fusion **45**, 337 (2005).